Low-temperature thermochronology and its geological significance in the central-northern section of the western margin of the Ordos Basin

Guangyuan Xing [1, 2], Zhanli Ren[1, 2*], Kai Qi [1, 2], Sasa Guo [1, 2], Yanzhao Liu [1, 2], Ying Zhang [3], Huaping Lan[4]

[1] *Department of Geology, Northwest University, Xi'an 710069, China;*

[2] *State Key Laboratory of Continental Evolution and Early Life;*

[3] *Reseach Institute of Yanchang Petroleum(Group) Co.Ltd., Xi'an 710075, China;*

[4] *Research Institute No. 203 of Nuclear Industry, Xi'an 710000, China*

Correspondence to: Zhanli Ren

E-mail: renzhanl@nwu.edu.cn

Abstract: The study of low-temperature thermochronology at plate edges provides favorable constraints for regional tectonic evolution and surface processes. Based on the existing thermochronological data of multiple cooling events since the Mesozoic era, we conducted apatite fission-track and apatite (U-Th)/He studies on drilling samples from the central-northern section of the western margin of the Ordos Basin, revealing the exhumation, cooling history and differences in the study area. The new thermal history simulation results show that the Zhuozishan Mountain (Mt.) region (ZM region) experienced large-scale exhumation in the Late Jurassic (160 Ma-150 Ma), with an average exhumation rate of ca. 45 m/Ma and an average cooling rate of ca. 2 ℃/Ma, slow exhumation at Early Cretaceous - Oligocene (130 Ma-30 Ma), with an average exhumation rate of ca. 10 m/Ma and an average cooling rate of ca. 1℃/Ma, and severe exhumation after Oligocene (30 Ma-), with an average exhumation rate of ca. 30 m/Ma and an average cooling rate

设置格式[残留的、余温]: 字体颜色: 自动设置

删除[残留的、余温]: **and**

删除[残留的、余温]: *State Key Laboratory of Continental Dynamics, Northwest University, Xi'an 710069, China;*

设置格式[残留的、余温]: 字体颜色: 自动设置

删除[残留的、余温]: fission track

删除[残留的、余温]: middle and northern parts of the western margin of the Ordos Basin

删除[残留的、余温]: uplift

删除[残留的、余温]: and

删除[残留的、余温]: middle and northern parts of the western margin of the Ordos Basin

删除[残留的、余温]: part

删除[残留的、余温]: uplift

设置格式[残留的、余温]: 字体颜色: 自动设置

设置格式[残留的、余温]: 字体颜色: 自动设置

删除[残留的、余温]: uplift

设置格式[残留的、余温]: 字体颜色: 自动设置

设置格式[残留的、余温]: 字体颜色: 自动设置

删除[残留的、余温]: uplift

设置格式[残留的、余温]: 字体颜色: 自动设置

of ca. 1.2 ℃/Ma; The Taole - Hengshanbao region (TH region) began to exhumation at Late Jurassic - Early Cretaceous (155 Ma-145 Ma), with an average exhumation rate of ca. 48 m/Ma and an average cooling rate of ca. 2.4 ℃/Ma, slowly exhumation at Early Cretaceous - Oligocene (145 Ma-30 Ma), with an average exhumation rate of ca. 7.5 m/Ma and an average cooling rate of ca. 0.3 ℃/Ma, and then violently exhumation, with an average exhumation rate of ca. 25 m/Ma and an average cooling rate of ca. 1 ℃/Ma; The Majiatan - Huianbao region (MH region) experienced large-scale exhumation at Late Jurassic - Early Cretaceous (158 Ma-137 Ma), with an average exhumation rate of ca. 45 m/Ma and an average cooling rate of ca. 1.8 ℃/Ma, with a slightly slower exhumation rate at 137 Ma-110 Ma, with an average exhumation rate of ca. 13 m/Ma and an average cooling rate of ca. 0.52 ℃/Ma, and entered a severe exhumation stage again at Late Cretaceous - Eocene (70 Ma-50 Ma), with an average exhumation rate of ca. 37.5 m/Ma and an average cooling rate of ca. 1.5 ℃/Ma. The Late Jurassic tectonic exhumation indicated by thermochronology corresponds to the formation of the western margin thrust fold structure, with the northern and southern sections starting earlier and the central section starting slightly later. At the same time, the exhumation time of different fault blocks decreases gradually from the edge of the basin to the interior of the basin, in the east-west direction. This is related to the different tectonic evolution and

设置格式[残留的、余温]: 字体颜色: 自动设置
删除[残留的、余温]: part
删除[残留的、余温]: uplift
设置格式[残留的、余温]: 字体颜色: 自动设置
设置格式[残留的、余温]: 字体颜色: 自动设置
删除[残留的、余温]: uplifted
设置格式[残留的、余温]: 字体颜色: 自动设置
设置格式[残留的、余温]: 字体颜色: 自动设置
删除[残留的、余温]: uplifted
设置格式[残留的、余温]: 字体颜色: 自动设置
设置格式[残留的、余温]: 字体颜色: 自动设置
删除[残留的、余温]: part
删除[残留的、余温]: uplift
设置格式[残留的、余温]: 字体颜色: 自动设置
设置格式[残留的、余温]: 字体颜色: 自动设置
删除[残留的、余温]: uplift
设置格式[残留的、余温]: 字体颜色: 自动设置
设置格式[残留的、余温]: 字体颜色: 自动设置
删除[残留的、余温]: uplift
设置格式[残留的、余温]: 字体颜色: 自动设置
设置格式[残留的、余温]: 字体颜色: 自动设置
删除[残留的、余温]: uplift
设置格式[残留的、余温]: 字体颜色: 自动设置
设置格式[残留的、余温]: 字体颜色: 自动设置
删除[残留的、余温]: middle
设置格式[残留的、余温]: 字体颜色: 自动设置

stress in their location.

Keyword： Ordos Basin； North China Block； Plate convergence； Low-temperature thermochronology； Yanshanian orogeny

1 Introduction

The North China Craton, as one of the oldest cratons in the world, has a long history spanning 3.8 billion years (Zhai, 2010; Zhang et al., 2018). Having undergone prolonged and complex tectonic evolution, it records nearly all major tectonic events from ancient to the present, especially preserving multi-phase evolutionary remnants since 1.8 Ga years (Peng et al., 2022). The Ordos Block is part of the North China Craton and one of its core geological units (Bao et al., 2019; Zhai, 2021). The present-day Ordos Basin, in a narrow sense, is located in the western part of the North China Craton, and has been developed since the Mesozoic as a residual intra-cratonic basin (Ren et al., 1995; Zhai, 2021). This basin is superimposed on a large Paleozoic basin, making it a composite basin (Liu et al., 2005). The Ordos Basin preserves the most complete sedimentary strata in North China Craton, including the Archaean, Proterozoic, Paleozoic, Mesozoic, and Cenozoic strata, and is rich in various energy and mineral resources such as oil, gas, coal, and uranium deposits.The thrust belt along the western margin of the Ordos Basin spans between tectonic blocks with different characteristics, including the North China Craton, the Alxa Block, the Central Asian

删除[残留旳、余温]: , and the differences in uplift rate and time may be related to the impact of multiple Yanshanian orogeny on the region.

删除[残留旳、余温]:

设置格式[残留旳、余温]: 缩进: 悬挂缩进: 1 字符

删除[残留旳、余温]: billion

删除[残留旳、余温]: ago

删除[残留旳、余温]: .

设置格式[残留旳、余温]: 字体:（默认）Times New Roman, 四号, 字体颜色: 自动设置

设置格式[残留旳、余温]: 字体颜色: 自动设置

删除[残留旳、余温]: It was formed on the foundation of the North China Craton through multiple phases of transformation, particularly since the Mesozoic, eventually developing into a residual intracratonic basin

设置格式[残留旳、余温]: 字体:（默认）Times New Roman, 四号, 字体颜色: 自动设置

设置格式[残留旳、余温]: 字体颜色: 自动设置

删除[残留旳、余温]: The Ordos Basin contains the most complete sedimentary strata in the North China region and is rich in multiple energy resources, including oil, gas, coal, and uranium, making it a highly resource-abundant basin.

删除[残留旳、余温]: spans across different tectonic units

Orogenic Belt, the Qinling Orogenic Belt, and the northeastern edge of the Tibetan Plateau (Fig.1). It is one of the regions with the most intense tectonic deformation within the Chinese mainland since the Mesozoic, recording numerous intracontinental deformation and orogenic events since the Mesozoic.

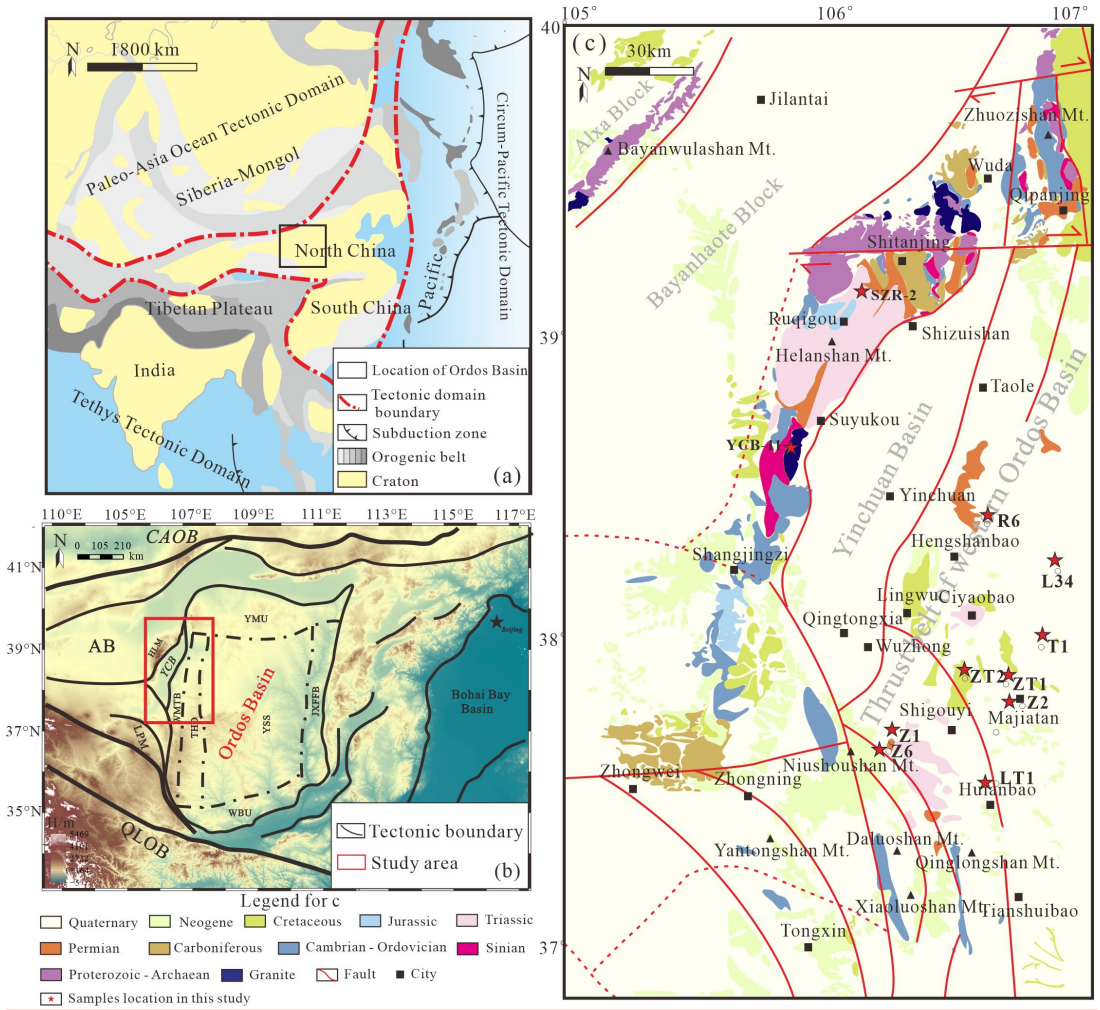

Fig.1 (a) Tectonic setting of China (modified from Peng et al., 2019), (b) Digital elevation model of the Ordos basin and surrounding areas. The red rectangle is the research area of this article (modified from Qi et al., 2024), abbreviation: AB, Alxa Block; CAOB, Central Asian Orogen Belt; HLM, Helanshan Mountain; JXFFB, Jinxi Fault-Fold Belt; LPM, Liupan Mountain; QLOB, Qinling Orogen Belt; THD, Tianhuan Depression; WMTB, Western Margin Thrust Belt; WBU, Weibei Uplift; YCB, Yinchuan Basin; YMU, Yimeng Uplift; YSS, Yishan Slope. (c) Geological map of the central-northern section of the western margin of the Ordos Basin (modified from Ma, 2019) and the sample locations in this study.The study area is located in

删除[残留旳、余温]: Phanerozoic

删除[残留旳、余温]: Additionally, the western margin of the Ordos Basin lies in the northern segment of the North-South Tectonic Belt of China, connecting different tectonic units between the western and eastern parts of northern China (Dong et al., 2021).

设置格式[残留旳、余温]: 居中, 缩进: 首行缩进: 0 字符

设置格式[残留旳、余温]: 缩进: 首行缩进: 8.5 毫米

删除[残留旳、余温]:

设置格式[残留旳、余温]: 字体颜色: 自动设置

the central-northern section of the western margin of the Ordos Basin (Fig. 1). Influenced by multiple tectonic movements, the region has a complex evolutionary history, with several large-scale, nearly north-south-oriented faults. In general, it can be considered that the structural style of the central-northern section of the western margin of the Ordos Basin is the result of the interaction between adjacent blocks. Over the years, previous published papers investigated the structural characteristics and properities of the central-northern section of the western margin of the Ordos Basin (Yang et al., 1986; Tang et al., 1988, 1992; Gan et al., 1990; Liu et al., 1995; Zhao et al., 1990), its formation mechanisms (Liu et al., 1997; Liu et al., 2005; Ouyang et al., 2012; Yang et al., 2011; Yang et al., 2006, 2008; Zhao et al., 2003, 2006, 2007a, c), and provenance (Jiang et al., 2019). Regarding the overall exhumation process along the western margin of the Ordos Basin, previous published papers based on the apatite fission-track method suggest that the exhumation in the southern section of the western margin of the Ordos Basin began in the Middle to Late Jurassic (Chen et al., 1999, 2007; Gao et al., 2000; Zhang et al., 2000; Zhao et al., 2003, 2006, 2007b; Zhao et al., 2017; Li et al., 2019; Ma et al., 2019; Peng Heng, 2020; Tian et al., 2023). In the central-northern section of the western margin of the Ordos Basin, low-temperature thermochronology studies are relatively scarce and have mainly focused on the Helanshan Mt. area (Ma et al., 2019;

删除[残留旳、余温]: thrust

删除[残留旳、余温]: the northern part of this tectonic belt is believed to result from interactions between adjacent tectonic blocks.

删除[残留旳、余温]: various scholars have conducted extensive research on the structural characteristics and properties

删除[残留旳、余温]: northern section of the western margin

删除[残留旳、余温]: uplift

设置格式[残留旳、余温]: 字体颜色: 自动设置

删除[残留旳、余温]: many scholars, using

删除[残留旳、余温]: fission track

删除[残留旳、余温]: s,

删除[残留旳、余温]: uplift

设置格式[残留旳、余温]: 字体颜色: 自动设置

删除[残留旳、余温]: Due to the presence of an east-west transfer zone in the Qingtongxia-Majiatan area, the western margin can be divided into three distinct tectonic systems: southern, central, and northern, based on differences in structural characteristics and sedimentation (Zhao et al., 2006).

删除[残留旳、余温]: northern part of the western margin

删除[残留旳、余温]: including the Helanshan Mt. region,

Zhao et al., 2007a; Liu, 2010), the Zhuozishan Mt. region (Zhuo, 2015; Li, 2006), the Shigouyi area (Gao, 2014; Zhao et al., 2007b, c; Ma et al., 2019; Li, 2019), drilling wells such as LC1, T1, and TS1 (Ren et al., 1995) (Fig.2).

On the basis of the limited published thermochronological data (Ma et al., 2019; Zhao et al., 2007a; Liu, 2010; Zhuo, 2015; Li, 2006; Gao, 2014; Zhao et al., 2007b, c; Ma et al., 2019; Li, 2019; Ren et al., 1995), it is evident that the study area recorded an exhumation event during the Mesozoic, but its timing and rate vary across different regions. The structural differences between the basin margin and the inner part have not been well clarified. Current research lacks a comprehensive perspective and does not provide a systematic understanding of tectonic events in the central-northern section of the western margin of the Ordos Basin since the Mesozoic. This greatly limits further insights into the overall tectonic evolution of the area and poses significant challenges for deeper research into intracontinental deformation in the basin and its surrounding regions.

This study applied low-temperature thermochronology methods, combined with thermal history modeling and field observation, to precisely constrain the exhumation and cooling history of the central-northern section of the western margin of the Ordos Basin. The research helps to improve our understanding of the evolution and tectonic

删除[残留的、余温]: 38°N Tectonic Belt
删除[残留的、余温]: and adjacent areas
删除[残留的、余温]: and
删除[残留的、余温]: LS1
删除[残留的、余温]: well
删除[残留的、余温]: well
删除[残留的、余温]: well
设置格式[残留的、余温]: 字体颜色: 自动设置
删除[残留的、余温]: From
设置格式[残留的、余温]: 字体颜色: 自动设置
删除[残留的、余温]: entered an uplift evolution stage
删除[残留的、余温]: but the timing and rate of uplift
删除[残留的、余温]: interior
删除[残留的、余温]: utilizes
删除[残留的、余温]: existing geological evidence
删除[残留的、余温]: uplift
设置格式[残留的、余温]: 字体颜色: 自动设置

processes in this region since the Mesozoic. Additionally, it offers a foundational reference for future oil and gas exploration efforts in the western margin of the basin.

2 Geological setting

The Ordos Basin, as one of the key geological element of the North China Craton, is a large basin formed during different periods and geodynamic settings (Ren et al., 2020). The evolution of the basin can be divided into several stages: Archean-Paleoproterozoic basement formation; Mesoproterozoic - Neoproterozoic rift basin development; early Palaeozoic stable continental margin sedimentation; late Palaeozoic to Middle Triassic intracratonic basin evolution; Late Triassic to Jurassic intracontinental depression basin evolution; Early Cretaceous westward contraction of the depression basin; Late Cretaceous to Cenozoic basin exhumation; formation of Cenozoic fault-depression basins in the surrounding areas (Liu et al., 2006; Ren et al., 2020;Li, 2006).

In order to define more precisely the differences in exhumation and cooling stages since the Mesozoic era, this article further divides the research area into the ZM region, the TH region, and the MH region.

删除[残留的、余温]: , providing important evidence for studying the formation and evolution of the Ordos Basin and the tectonic deformation that occurred along the basin's margins during the Mesozoic.

删除[残留的、余温]: units

删除[残留的、余温]: composite

删除[残留的、余温]: , across varying extents, and under diverse

删除[残留的、余温]: Based on the basin types and tectonic evolutionary characteristics of different eras, the basin’s evolution can be divided into

删除[残留的、余温]: stage,

删除[残留的、余温]: stage,

删除[残留的、余温]: Early Paleozoic

删除[残留的、余温]: stage,

删除[残留的、余温]: L

删除[残留的、余温]: L

删除[残留的、余温]: Paleozoic

删除[残留的、余温]: stage,

删除[残留的、余温]: stage,

删除[残留的、余温]: ,

删除[残留的、余温]: significant

删除[残留的、余温]: uplift

删除[残留的、余温]: ,

删除[残留的、余温]: F

删除[残留的、余温]: In order to more precisely define the differences in the later uplift and cooling processes,

删除[残留的、余温]: Zhuozishan Mt. Part

删除[残留的、余温]: Taole-Hengshanbao part

删除[残留的、余温]: Majiatan-Huianbao part.

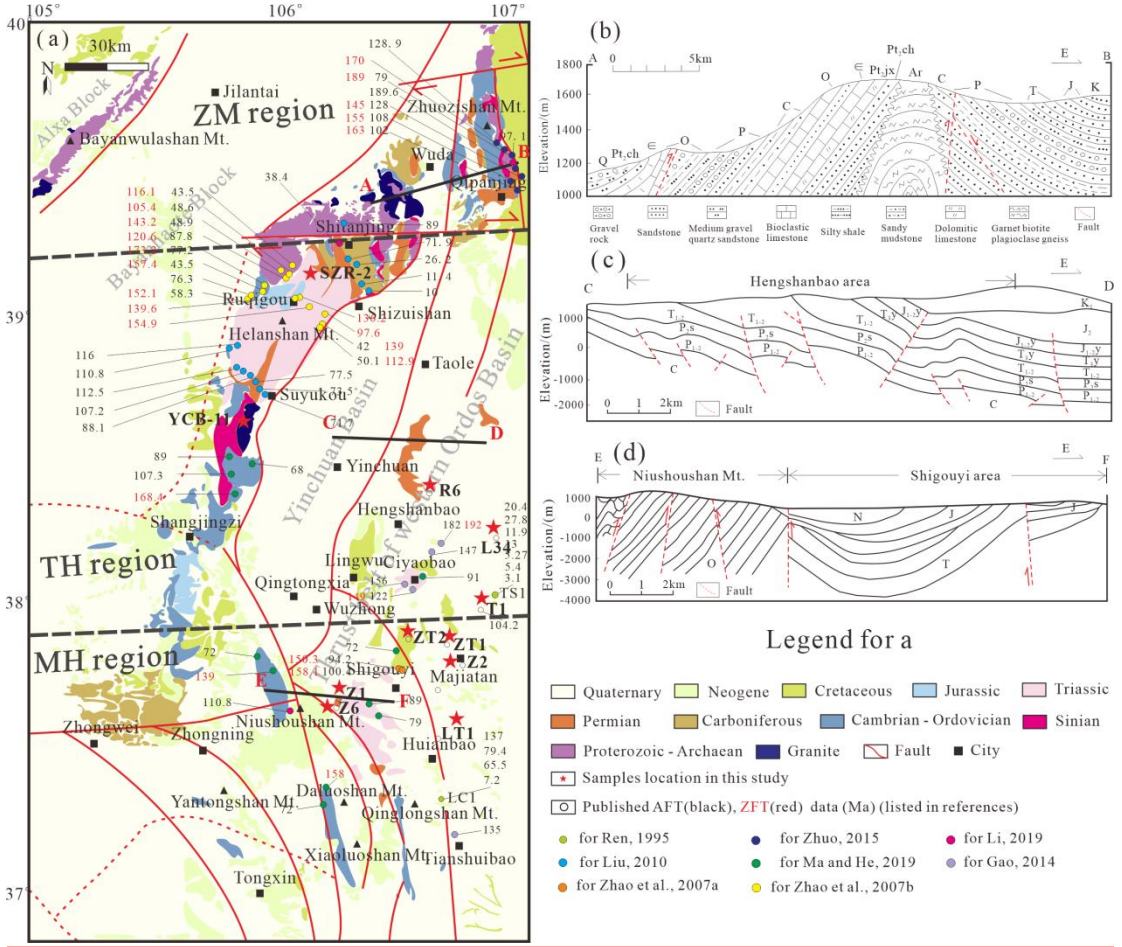

Fig. 2 (a) Compilation of previously published low-temperature thermochronological data in the study area, (b-d) W-E oriented simplified geological cross-sections (modified from Xing et al., 2024; Liu et al., 2024, and Ma et al., 2019, respectively).

In the ZM region, the main body is the Zhuozishan anticline, with an east-west length of about 20km. The core of the anticline exposes older strata, with Archean granitic gneiss of the Qianlishan Group at its core. Moving westward, it sequentially exposes the Changcheng System Huangqikou Formation, Jixian System Wangquankou Formation, Cambrian Taosigou Formation, Hulusitai Formation, Zhangxia Formation, Abuqiehai Formation, Ordovician Sandaokan Formation, Zhuozishan Formation, and the Permian Shanxi Formation and Shihezi Formation, and exposes the Carboniferous, Permian, Triassic, Jurassic, and

设置格式[残留的、余温]: 居中, 缩进: 左 -0.95 字符,
设置格式[残留的、余温]: 字体:（默认）Times New Ro
设置格式[残留的、余温]: 字体:（默认）Times New Ro
设置格式[残留的、余温]: 字体:（默认）Times New Ro
设置格式[残留的、余温]: 字体:（默认）Times New Ro
设置格式[残留的、余温]: 字体:（默认）Times New Ro
删除[残留的、余温]:
设置格式[残留的、余温]: 字体: 小四, 字体颜色: 自动
设置格式[残留的、余温]: 字体颜色: 自动设置
删除[残留的、余温]: Fig.1 (a) Tectonic setting of China
设置格式[残留的、余温]: 图案: 清除(自动设置), 字体
设置格式[残留的、余温]: 字体颜色: 自动设置
删除[残留的、余温]: Zhuozishan Mt. Part
设置格式[残留的、余温]: 字体:（默认）Times New Ro
设置格式[残留的、余温]: 字体颜色: 自动设置
删除[残留的、余温]: faults thrust from west to east,

Cretaceous strata in sequence towards the east (Fig. 2b) (Zhuo, 2015; Xing et al., 2024).In the TH region, the faults in this area exhibit high-angle thrusting from east to west, characterized by a series of imbricated thrust faults (Fig. 2c). In the MH region, four west-dipping thrust faults develop from west to east. From west to east, the Weizhou fault zone, Qinglongshan fault zone, Shigouyi fault zone, and Yandunshan fault zone have formed in sequence. Among them, the Shigouyi fault zone, in an syncline form, is situated between the Qingshanlong Fault and the Huianbao-Shajingzi Fault (Fig. 2d).

3 Sampling strategy and methodology

3.1 Previous thermochronological data

This study collected a total of 85 published low-temperature thermochronology data from the western margin of the Ordos Basin, specifically from the area between the Zhuozishan Mt. and the Tianshuibao city, including 62 apatite fission-track ages and 23 zircon fission-track ages (Fig. 3). Samples with higher mineral closure temperatures exhibit older apparent ages. The ages obtained through the apatite fission-track analysis range from 189.6 Ma to 3.1 Ma, while zircon fission-track ages range from 192 Ma to 105.4 Ma. These findings indicate a long cooling history and a complex exhumation process in the study area. Based on the collected data, we plotted histograms and kernel density estimation curves, revealing that the density peaks for apatite and

删除[残留的、余温]: 1d
设置格式[残留的、余温]: 字体颜色: 自动设置
删除[残留的、余温]:
删除[残留的、余温]: structural characteristics differ fr
删除[残留的、余温]: 1e
设置格式[残留的、余温]: 字体颜色: 自动设置
删除[残留的、余温]: Additionally, this part corresponds
删除[残留的、余温]: ing
删除[残留的、余温]: These faults exhibit steep upper an
删除[残留的、余温]: the major thrust sheets include
删除[残留的、余温]: thrust sheet
删除[残留的、余温]: thrust sheet
删除[残留的、余温]: thrust sheet
删除[残留的、余温]: thrust sheet.
删除[残留的、余温]: thrust sheet
删除[残留的、余温]: thrust sheet
删除[残留的、余温]: anticlinal
删除[残留的、余温]: pu
删除[残留的、余温]: 1f
设置格式[残留的、余温]: 字体颜色: 自动设置
删除[残留的、余温]: In the Hengshanbao area, east-dipp
删除[残留的、余温]: fission track
删除[残留的、余温]: fission track
删除[残留的、余温]: 2
设置格式[残留的、余温]: 字体颜色: 自动设置
删除[残留的、余温]: The ages of apatite samples
删除[残留的、余温]: 3.1 Ma to 189.6 Ma
删除[残留的、余温]: fission track
删除[残留的、余温]: 105.4 Ma to 192 Ma
删除[残留的、余温]: uplift
设置格式[残留的、余温]: 字体颜色: 自动设置
删除[残留的、余温]: fission tracks

zircon are at 78 and 101 Ma, and at 153 Ma respectively (Fig.3).

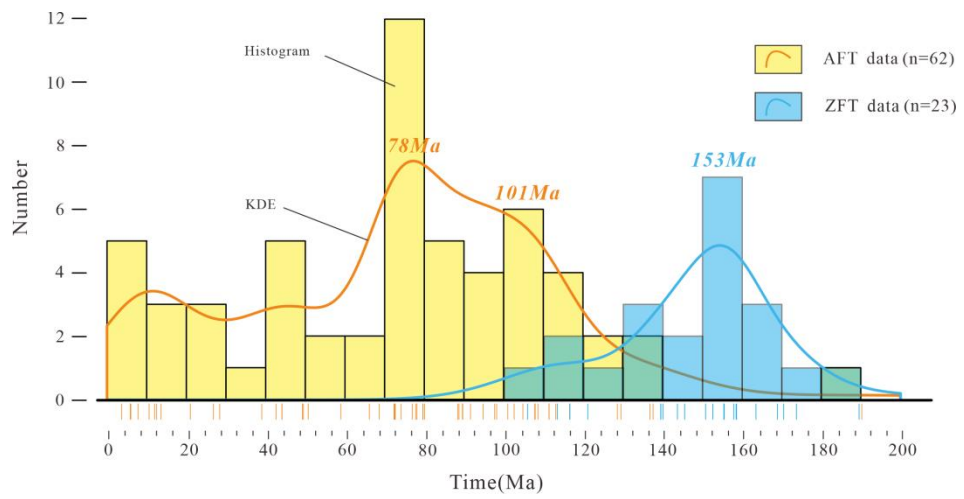

Fig.3 Histogram and kernel density estimation (KDE) plot of published thermochronological data in the study area.

In summary, previous thermochronological data indicate that multiple cooling events have occurred in the region since the Mesozoic era (Ren et al., 1995; Zhao et al., 2007a, b; Liu, 2010; Zhuo, 2015; Gao, 2014; Li, 2019; Ma et al., 2019). Due to the lack of thermochronological techniques such as the (U-Th)/He method and the existence of regional differences in the study area, the cooling history of the study area after the Mesozoic has not been systematically constrained.

3.2 Sample collection and experimental methods

This study applies low-temperature thermochronological methods to constrain the spatiotemporal evolution of the upper few kilometers of the lithosphere. Apatite fission-track analysis is sensitive to temperature variations in the range of 60 °C to 120 °C (the partial annealing zone), while apatite (U-Th)/He dating is suitable for defining the

删除[残留的、余温]: fission tracks

删除[残留的、余温]: Ma,

删除[残留的、余温]: ,

设置格式[残留的、余温]: 字体颜色: 自动设置

删除[残留的、余温]: 2

设置格式[残留的、余温]: 字体颜色: 自动设置

删除[残留的、余温]: geochronological dates in the central-northern section of the western margin of the Ordos Basin.

删除[残留的、余温]: The bandwidth and bin width are both set to 10 Ma for all plots when the graph is drawn.

设置格式[残留的、余温]: 字体:（默认）Times New Roman, （中文）宋体, 四号, 字体颜色: 自动设置

删除[残留的、余温]: However, due to a lack of chronological methods, the cooling history of the study area during the late Cenozoic has not been well constrained.

设置格式[残留的、余温]: 字体颜色: 自动设置

删除[残留的、余温]: thermochronology

删除[残留的、余温]: As one of the most widely used and effective thermochronological methods (Gleadow and Seiler, 2015; Peng, 2020),

删除[残留的、余温]: apatite

删除[残留的、余温]: fission track

time-temperature history in the range of 40 °C to 75 °C (Ketcham, 2005; Gallagher, 2012; Flowers et al., 2015; Farley et al., 2002).

The author has previously conducted thermochronological studies in the ZM region （Xing et al., 2024）.To systematically study the differences in exhumation and cooling, the relationship between structural evolution at the basin edge and within the basin, and to address the current gaps in thermochronology in the research area, this study collected 13 valuable samples, including 11 core samples from 9 drilling wells and 2 field outcrop samples. The samples are well-distributed across the entire TH region and MH region (Fig.2a). Sample information was detailed in Table 1, and sample localities and sites were marked in Fig.1 and Fig.2.

Table 1 Sample information and summary of geochronology methods used.

Sample NO.	Formation	Lithology	Coordinate(N)	Coordinate(E)	Methods
YCB-11	Ar	Granodiorite	38°25'59.9"	106°5'55.8"	AFT
SZR-2	T_3	Sandstone	39°0'27.7"	106°9'15.9"	AFT
W22L34-21	P_1	Sandstone	38°7'19.3"	107°6'3.2"	AFT
W22R6-6	P_2	Sandstone	38°15'29.1"	106°45'50.1"	AFT
W22R6-7	P_2	Sandstone	38°15'29.1"	106°45'50.1"	AFT
W22T1-5	J_2	Sandstone	38°1'3.7"	107°5'9.1"	AFT
W22Z1-33	J_2	Sandstone	37°40'36.2"	106°24'4.6"	AFT, AHe
W22Z1-34	J_2	Sandstone	37°40'36.2"	106°24'4.6"	AFT
W22Z2-11	P_2	Sandstone	37°46'51.1"	106°56 '7.4"	AFT
W22ZT1-44	T_3	Sandstone	37°50'37.4"	106°53'41.2"	AFT
W22ZT2-18	J_2	Sandstone	37°51'53.1"	106°46'53.2"	AHe
W22Z6-16	P_1	Sandstone	37°36'45.3"	106°23'14"	AFT
W22LT1-20	P_1	Sandstone	37°27'8.2"	106°47'8.7"	AFT

After obtaining the samples, apatite was separated using conventional heavy liquid and magnetic separation methods. All 13 samples were analyzed using apatite fission-track (AFT) methodology.

设置格式[残留的、余温]: 字体:（默认）Times New Ro
设置格式[残留的、余温]: 字体:（默认）Times New Ro
设置格式[残留的、余温]: 字体颜色: 自动设置
删除[残留的、余温]: uplift
设置格式[残留的、余温]: 字体颜色: 自动设置
删除[残留的、余温]: in the central-northern part of the
删除[残留的、余温]: 6
设置格式[残留的、余温]: 字体颜色: 自动设置
删除[残留的、余温]: 5
设置格式[残留的、余温]: 字体颜色: 自动设置
删除[残留的、余温]: Apatite fission track analysis and
设置格式[残留的、余温]: 字体:（默认）Times New Ro
删除[残留的、余温]: central-northern region of the west
设置格式[残留的、余温]: 字体颜色: 自动设置
设置格式[残留的、余温]: 居中, 缩进: 首行缩进: 8.5 毫米
设置格式[残留的、余温]: 字体: 小五
设置格式[残留的、余温]: 字体: 小五
设置格式[残留的、余温]: 字体: 小五
设置格式[残留的、余温]: 字体: 小五
设置格式[残留的、余温]: 字体: 小五
设置格式[残留的、余温]: 字体: 小五
设置格式[残留的、余温]: 字体: 小五
设置格式[残留的、余温]: 字体: 小五
设置格式[残留的、余温]: 字体: 小五
设置格式[残留的、余温]: 字体: 小五
设置格式[残留的、余温]: 字体: 小五
删除[残留的、余温]:
设置格式[残留的、余温]: 字体: 小四, 字体颜色: 自动
设置格式[残留的、余温]: 字体颜色: 自动设置
删除[残留的、余温]: 6
设置格式[残留的、余温]: 字体颜色: 自动设置
删除[残留的、余温]: fission track

After selecting mineral grains, the samples were prepared, tested, and analyzed at the Petroleum Thermochronology Laboratory in the Department of Geology at Northwest University. The calculation method for AFT ages follows Hasebe et al. (2004), and ages were analyzed using RadialPlotter software (Vermeesch, 2009). Additionally, the HeFTy software was utilized to simulate the cooling history (Ketcham, 2005).

Additionally, following three criteria — crystalline integrity of the automorphic particles, the purity of the particles, and ensuring that the crystal dimensions perpendicular to the c-axis exceed 60-70 μm — apatite grains from samples Z1-33 and ZT2-18 were chosen under a high magnification (160x) binocular microscope for (U-Th)/He (AHe) dating. The dating was conducted at the Ar-Ar and (U-Th)/He Geochronology Laboratory of the Institute of Geology and Geophysics, Chinese Academy of Sciences.

Due to the complexity of annealing processes, the measured apparent ages lack any practical geological significance (Flowers et al., 2015). By utilizing the measured ages, track lengths, angle with the C-axis of mineral particles, Dpar values, this thermal history can be inversely modeled (Ketcham, 2005). In this study, HeFTy version 1.6.7 software was used for inverse modeling (Ketcham, 2005), and the Ketcham (2005) multi-dynamic annealing model was selected for the

删除[残留旳、余温]: (Fig.3, 4a)

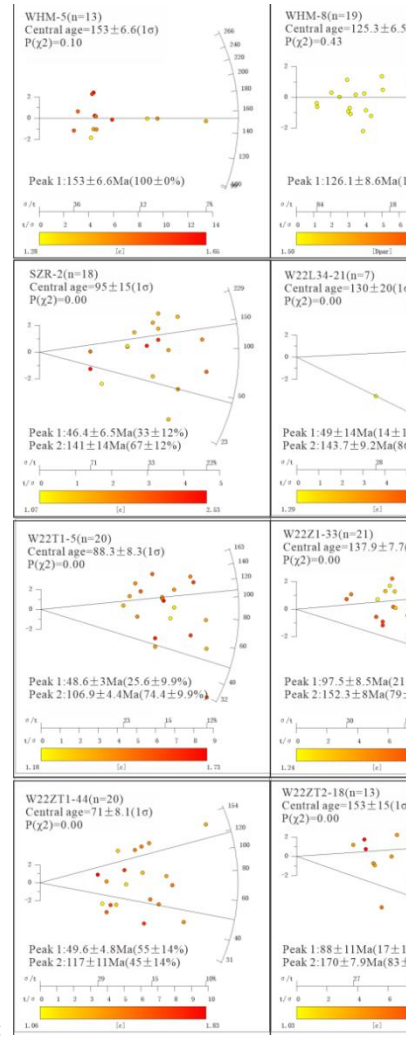

删除[残留旳、余温]:

删除[残留旳、余温]: Fig.3 AFT age Radial plots for samples (WHM-5, 8, and 12 are the data that the author will soon publish, while the rest are newly published data in this paper).

删除[残留旳、余温]: selecting well-formed, pure grains

删除[残留旳、余温]: μm

删除[残留旳、余温]: This experiment

删除[残留旳、余温]: Argon-Argon

删除[残留旳、余温]: U-Th-He

删除[残留旳、余温]: The thermal history of the samples was also modeled using HeFTy software (Ketcham, 2005).

inversion simulation, along with the corrected confined track lengths. The original confined track length was set at 16.3 μm, and the present-day surface temperature was 20°C. The goodness-of-fit parameter (GOF) was used to indicate how well the simulation results matched the actual measurements; a higher value signifies a better fit. When the GOF value obtained from the simulation exceeds 0.05, it indicates that the simulation results are acceptable, while a GOF value greater than 0.5 indicates a very good match. The simulated ages and lengths both had GOF values greater than 0.5 and close to 1, suggesting that the simulation results closely aligned with the measured values.

4 Results

4.1 Low-temperature thermochronology results

4.1.1 The TH region

The AFT central ages of the two samples from well R6 (R6-6 and R6-7) are 140.4±15.7 Ma and 115.3±10.2 Ma, with average track lengths of 11.66±1.02 μm and 12.1±1.52 μm, respectively. The AFT central age of the sample from well L34 (L34-21) is 130±19.8 Ma. In the Helanshan Mt. area, the AFT central ages of samples SZR-2 and YCB-11 are 95.2±14.8 Ma and 95.4±3.7 Ma, with average track lengths of 12.01±1.68 μm and 12.88±1.11 μm, respectively. The AFT central ages of these five samples in this region are significantly younger than the stratigraphic ages from which they were derived, indicating that the samples have

删除[残留的、余温]: **4.1.1 Zhuozishan Mt. part**
The AFT central ages of the three sandstone samples from the Zhuozishan Mt. part (WHM-5, WHM-8, WHM-12) are 153±6.6 Ma, 125±6 Ma, and 135±5 Ma, respectively, all of which are significantly younger than the stratigraphic ages from which the samples were derived. The average track lengths are 12.16±1.54 μm, 11.43±1.55 μm, and 13.3±1.7 μm, all of which are shorter than the spontaneous track original length of 16.3±0.9 μm, indicating that the samples have undergone annealing and cooling processes. All three samples passed the χ^2 test ($P(\chi^2) > 5\%$), suggesting that each sample contains a single age component. The RadialPlotter software provided single ages of 153±6.6 Ma, 126.1±8.6 Ma, and 134.7±7.9 Ma (Fig. 4b), which are consistent with the central ages within a certain error range. The age of 153±6.6 Ma may represents a tectonic event in the Late Jurassic, while 134.7±7.9 Ma may corresponds to an early tectonic event in the Early Cretaceous, and 126.1±8.6 Ma may indicates a tectonic event in the Late Early Cretaceous.

删除[残留的、余温]: **2**

设置格式[残留的、余温]: 字体颜色: 自动设置

删除[残留的、余温]: **Taole-Hengshanbao part**

undergone annealing and cooling processes. Only the YCB-11 sample passed the χ^2 test, with the RadialPlotter software providing a single peak age of 95.2±3.2 Ma. The remaining four samples did not pass the χ^2 test, suggesting that each sample contains at least two age populations. The RadialPlotter software (Vermeesch, 2009) was used to decompose the ages, and these peak ages record potential tectonic activities in this region from Late Jurassic to Eocene (Table 2, Fig. 4).

Table 2 Fission-track age obtained by the laser method

Sample	n	Ns	ρs(×10⁶/cm²)	^{238}U (×10⁻⁶)	Central age (Ma)	P (χ2) (%)	MTL(μm)(N)	Dpar (μm)
YCB-11	27	904	1.203	26.55±8.78	95.4±3.7	18	12.88±1.11 (97)	1.53±0.19
SZR-2	18	187	0.927	20.91±1.49	95.2±14.8	0	12.01±1.68 (43)	1.70±0.4
W22L34-21	7	269	1.04	16.27±3.41	130±19.8	0		1.43±0.17
W22R6-6	14	339	0.967	16.38±1.8	140.4±15.7	0	11.66±1.02 (35)	1.66±0.23
W22R6-7	26	852	0.946	19.20±1.52	115.3±10.2	0	12.1±1.52 (56)	1.44±0.16
W22T1-5	20	946	1.814	47.72±4.08	88.3±8.3	0	11.3±1.22 (78)	1.46±0.14
W22Z1-33	21	1066	1.547	24.52±1.75	137.9±7.7	0	10.89±1.15 (82)	1.61±0.24
W22Z1-34	15	826	2.182	34.22±2.77	144.5±12.2	0	10.75±1.13 (80)	1.42±0.16
W22Z2-11	12	502	0.794	8.60±2.53	189.5±11.1	5	12.21±1.31 (52)	1.48±0.21
W22ZT1-44	20	778	1.312	38.34±3.7	71.0±8.1	0		1.41＋0.2
W22ZT2-18	13	643	2.416	33.92±2.6	152.6±15.2	0		1.49±0.24
W22Z6-16	18	398	1.092	49.28±5.8	68.6±13.7	0		1.31±0.23
W22LT1-20	22	677	1.135	47.69±3.1	51.9±6.1	0	11.43±0.99 (50)	1.40±0.18

Note: n: number of measured grains; ρ s(Ns): spontaneous track densities (tracks numbers measured); P(%): probability of obtaining χ 2-test value, a probability >5% is indicative of a homogenous population; MTL: mean confined track lengths with c-axis correction.

Table 3 Borehole Z1 and ZT2 apatite (U-Th)/He data.

Sample	Mass(ug)	Rs (um)	U (ppm)	Th (ppm)	Th/U	[eU] (ppm)	mol ^{4}He	Std. mol ^{4}He	FT	Cor Age (Ma)	± σ (Ma)
W22Z1-33-A1	3.00	47.2	33.7	35.4	1.1	42.1	3.0575 E-14	3.7211E -16	0.7 09	63.48	3.38
W22Z1-33-A2	5.95	64.3	20.9	9.0	0.4	23.1	3.9018 E-14	4.8104E -16	0.7 88	67.06	3.58
W22Z1-	2.48	47.8	41.7	114.7	2.8	68.7	4.0084	8.5601E	0.7	61.64	3.43

删除[残留旳、余温]: during the Late Jurassic, early Earl
设置格式[残留旳、余温]: 字体颜色: 自动设置
删除[残留旳、余温]: c
设置格式[残留旳、余温]: 字体: 小四, 非加粗, 字体颜
设置格式[残留旳、余温]: 缩进: 首行缩进: 8.5 毫米,
设置格式[残留旳、余温]: 字体: 小四, 非加粗, 字体颜
设置格式[残留旳、余温]: 字体: 小四, 非加粗, 字体颜
带格式表格[残留旳、余温]
设置格式[残留旳、余温]: 字体: 小五
设置格式[残留旳、余温]: 字体: 小五
设置格式[残留旳、余温]: 字体: 小五
设置格式[残留旳、余温]: 字体: 小五
设置格式[残留旳、余温]: 字体: 小五
设置格式[残留旳、余温]: 字体: 小五
设置格式[残留旳、余温]: 字体: 小五
设置格式[残留旳、余温]: 字体: 小五
设置格式[残留旳、余温]: 字体: 小五
设置格式[残留旳、余温]: 字体: 小五
设置格式[残留旳、余温]: 字体: 小四, 字体颜色: 自动
设置格式[残留旳、余温]: 行距: 单倍行距, 孤行控制
带格式表格[残留旳、余温]
设置格式[残留旳、余温]: 字体: 小五
设置格式[残留旳、余温]: 字体: 小五
设置格式[残留旳、余温]: 字体: 小五

33-A3							E-14	-16	07		
W22ZT							7.6887	9.0770E	0.7		
2-18-A1	3.95	53.6	8.4	3.7	0.5	9.2	E-15	-17	46	52.61	2.82
W22ZT							4.2928	5.2774E	0.6		
2-18-A2	2.69	47.0	45.7	160.9	3.6	83.5	E-14	-16	98	50.69	2.66
W22ZT							1.2764	1.5287E	0.7		
2-18-A3	2.91	48.4	19.0	4.3	0.2	20.1	E-14	-16	23	56.31	3.17

Note:Rs, equivalent spherical radius; eU, effective uranium concentration; FT, α-ejection correction factor; Cor. Age, AHe age with α-ejection correction.

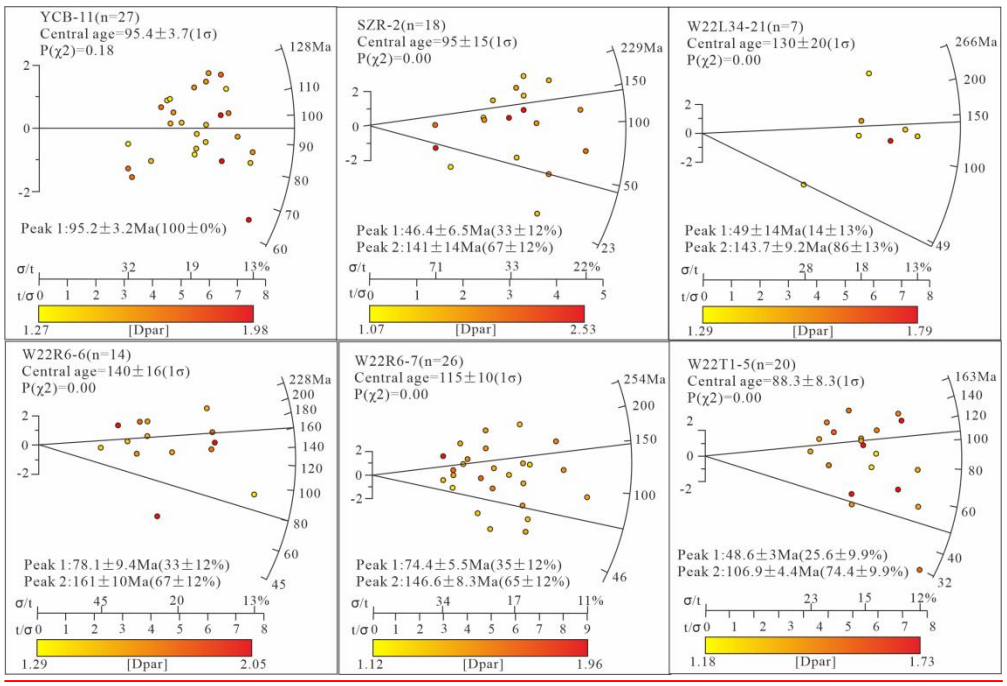

Fig.4 AFT age Radial plots for The TH region

设置格式[残留的、余温]: 字体: 小五
设置格式[残留的、余温]: 字体: 小五
设置格式[残留的、余温]: 字体: 小五
设置格式[残留的、余温]: 缩进: 首行缩进: 0 字符, 孤行控制
设置格式[残留的、余温]: 字体: 小四
设置格式[残留的、余温]: 字体: 小四
设置格式[残留的、余温]: 字体: 小四
设置格式[残留的、余温]: 字体: 小四
设置格式[残留的、余温]: 字体: 小四
设置格式[残留的、余温]: 字体: 小四
设置格式[残留的、余温]: 居中, 缩进: 首行缩进: 0 字符
设置格式[残留的、余温]: 居中, 缩进: 首行缩进: 8.5 毫米
设置格式[残留的、余温]: 字体: 小四, 非加粗

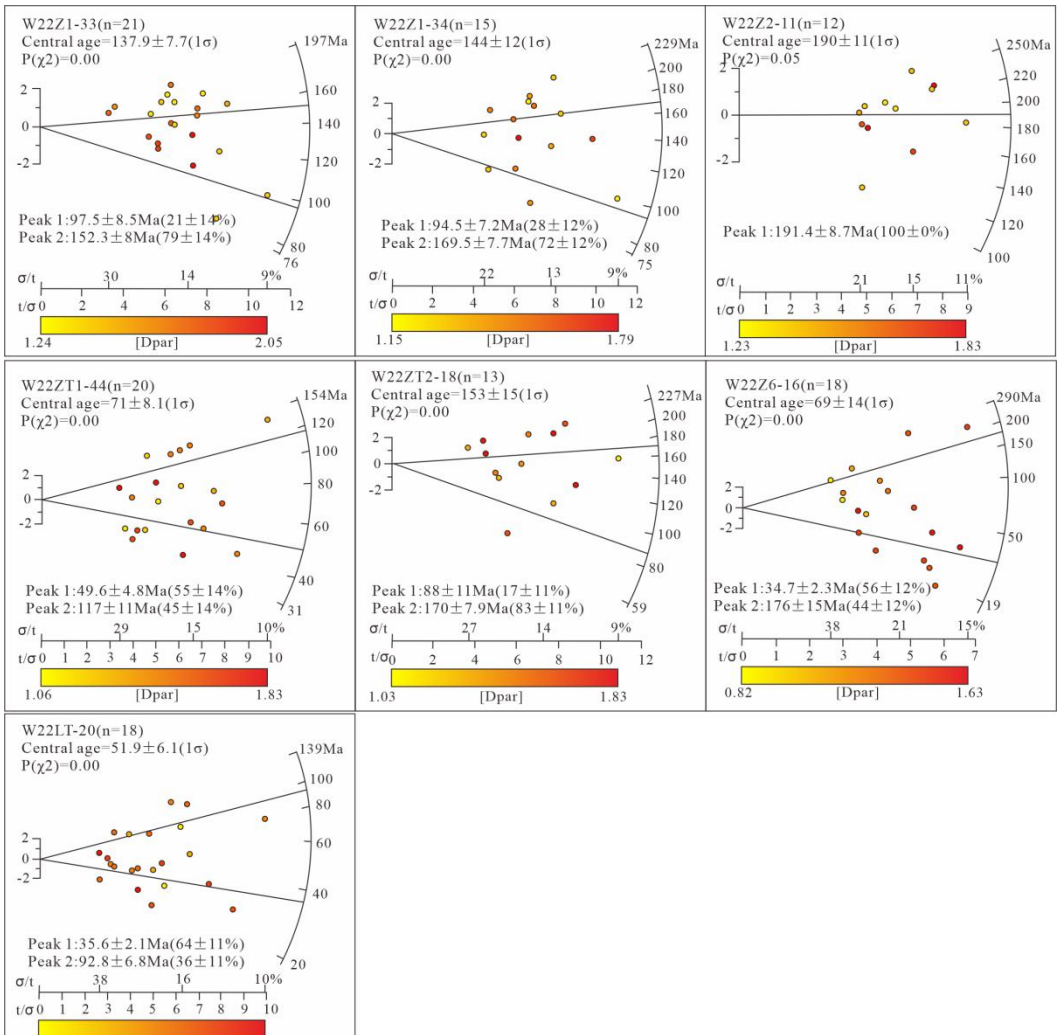

Fig.5 AFT age Radial plots for The MH region

4.1.2 The MH region

Due to this region being a key area for oil and gas exploration, a large number of drilling samples are available. Except for sample Z2-11, which passed the χ^2 test, the remaining samples did not pass the test. The fission-track ages obtained for this region range from 189.5 Ma to 35.6 Ma and were statistically divided into three peak values: 42 Ma, 95 Ma, and 170 Ma (Fig.5). All of these ages are significantly younger than the stratigraphic ages , indicating that they have undergone exhumation and

设置格式[残留的、余温]: 居中, 缩进: 首行缩进: 0 字符

设置格式[残留的、余温]: 字体: 小四, 字体颜色: 自动

设置格式[残留的、余温]: 居中, 缩进: 首行缩进: 0 字符

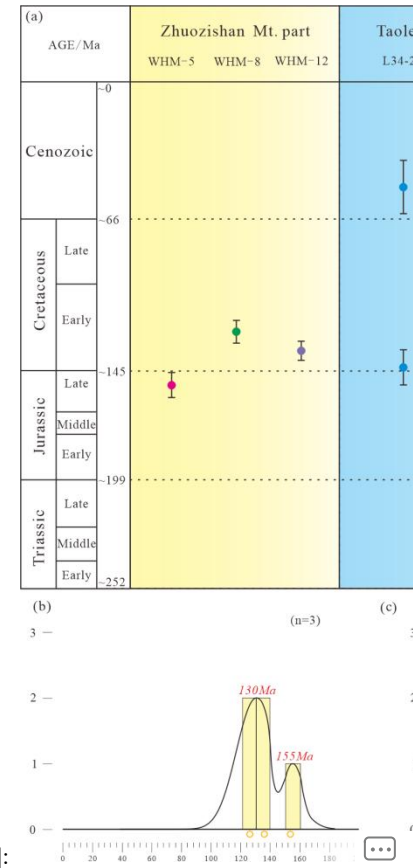

删除[残留的、余温]:

设置格式[残留的、余温]: 字体颜色: 自动设置

删除[残留的、余温]: **3**

设置格式[残留的、余温]: 字体颜色: 自动设置

删除[残留的、余温]: **Majiatan-Huianbao part**

删除[残留的、余温]: sweet spot

删除[残留的、余温]: The ages range from 35.6 to 189.5 Ma

设置格式[残留的、余温]: 字体颜色: 自动设置

删除[残留的、余温]: from which they were derived

删除[残留的、余温]: uplift

设置格式[残留的、余温]: 字体颜色: 自动设置

cooling processes. The three single-grain AHe ages for sample Z1-33 range from 61.64 Ma to 67.06 Ma, while the three single-grain AHe ages for sample ZT2-18 range from 50.69 Ma to 56.31 Ma, with no significant correlation to eU, recording late exhumation and cooling events (Table 3, Fig. 6).

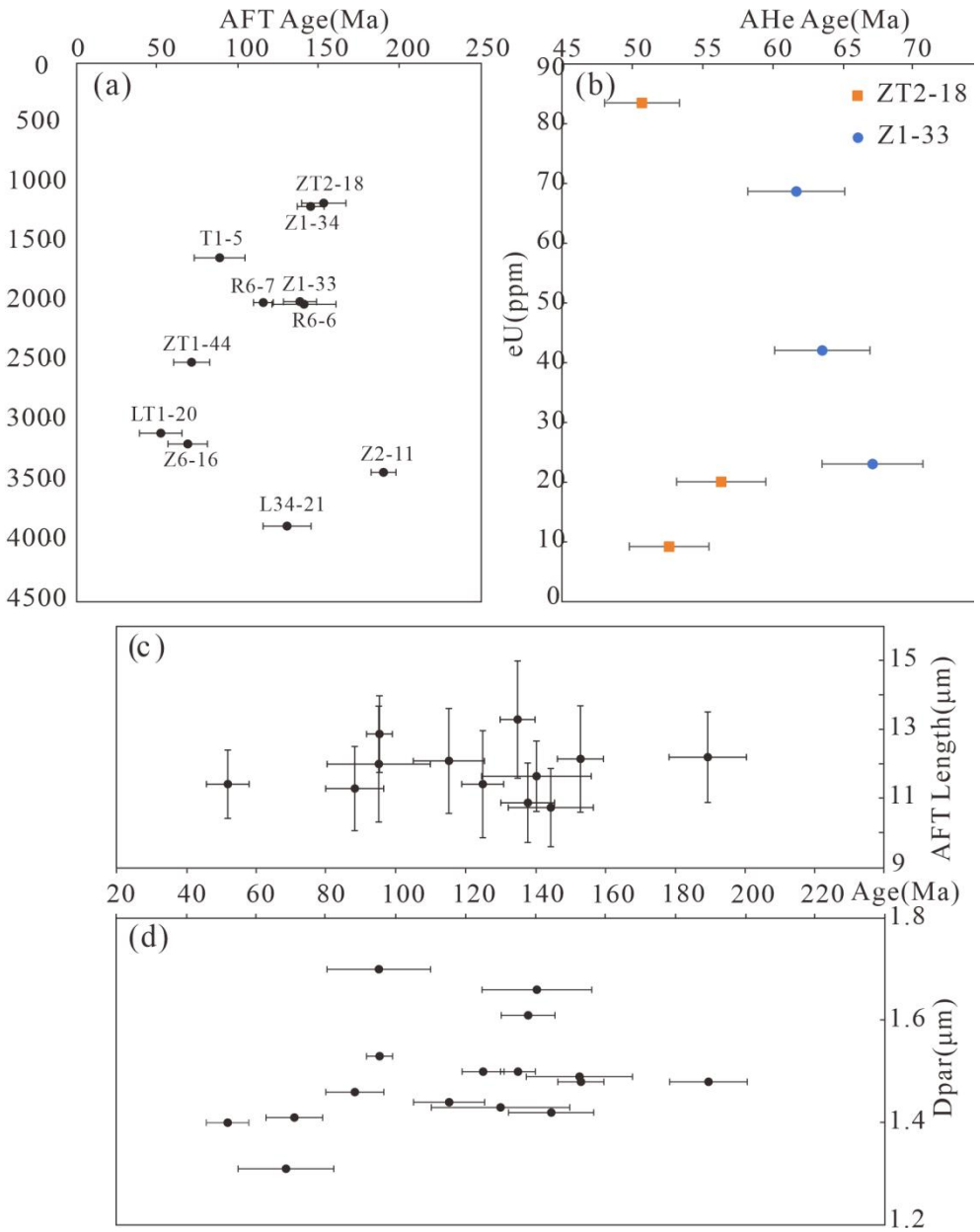

Fig. 6 (a) Relationships between AFT Age and depth; (b) Relationships between AHe age and eU; (c), Relationships between AFT Age and AFT length; (d) Relationships between AFT Age and Dpar.

In addition, the correlation between track length and AFT age

删除[残留的、余温]: (Fig. 4d)

删除[残留的、余温]: uplift

设置格式[残留的、余温]: 字体颜色: 自动设置

设置格式[残留的、余温]: 字体颜色: 自动设置

删除[残留的、余温]: 5

设置格式[残留的、余温]: 字体颜色: 自动设置

删除[残留的、余温]: 5

设置格式[残留的、余温]: 字体颜色: 自动设置

删除[残留的、余温]: Relationships between AFT Age and (a) depth, (c) AFT length, and (d) Dpar, (b) relationships between AHe age and eU.

indicates a complex cooling history in the region. Considering the different annealing dynamics (Ketcham et al., 2007), the chemical composition of the grains may influence the AFT age and length (Carlson et al., 1999; Barbarand et al., 2003). However, the Dpar values in the samples range from 1.31 μm to 1.70 μm, showing minimal variation and no significant correlation with the AFT ages. This suggests that the influence of chemical composition on AFT age is either minimal or nonexistent.

4.2. Thermal history modeling

Among the 13 samples, 12 with more extensive length information were selected for thermal history simulation, representing a broad distribution across the study area to assess their potential thermal history and determine their exhumation and cooling times. The goodness-of-fit parameters for both length and age in this simulation were above 0.90, indicating a good fit. The inverted time-temperature paths are shown in Fig. 7.

The modeling results indicate significant differences in the thermal histories of samples from different regions. Two samples from the western part of the TH region record a rapid exhumation event from 110 Ma to 90 Ma, followed by a long period of slow cooling, and finally a rapid cooling event around 25 Ma. The R6 well records a rapid cooling

删除[残留旳、余温]: Due to the complexity of annealing processes, the measured apparent ages lack any practical geological significance (Flowers et al., 2015). By utilizing the measured ages, track lengths, Dpar values, and other parameters, this thermal history can be inversely modeled (Ketcham, 2005). In this study, HeFTy version 1.6.7 was used for inverse modeling (Ketcham, 2005), in conjunction with all available low-temperature thermochronology data for path analysis. The Ketcham (2005) multi-dynamic annealing model was selected for the inversion simulation, along with the corrected confined track lengths. The original confined track length was set at 16.3 μm, and the present-day surface temperature was 20°C. The goodness-of-fit parameter (GOF) was used to indicate how well the simulation results matched the actual measurements; a higher value signifies a better fit. When the GOF value obtained from the simulation exceeds 0.05, it indicates that the simulation results are acceptable, while a GOF value greater than 0.5 indicates a very good match. The simulated ages and lengths both had GOF values greater than 0.5 and close to 1, suggesting that the simulation results closely aligned with the measured values.

history during the Late Cretaceous (ca. 155 Ma). The T1 well records a rapid exhumation event from 95 Ma to 85 Ma. In the MH region, the Z1 well simulation reveals rapid exhumation from 158 Ma to 137 Ma, and the three samples in this region show rapid exhumation between 70 Ma and 50 Ma (Fig.7).

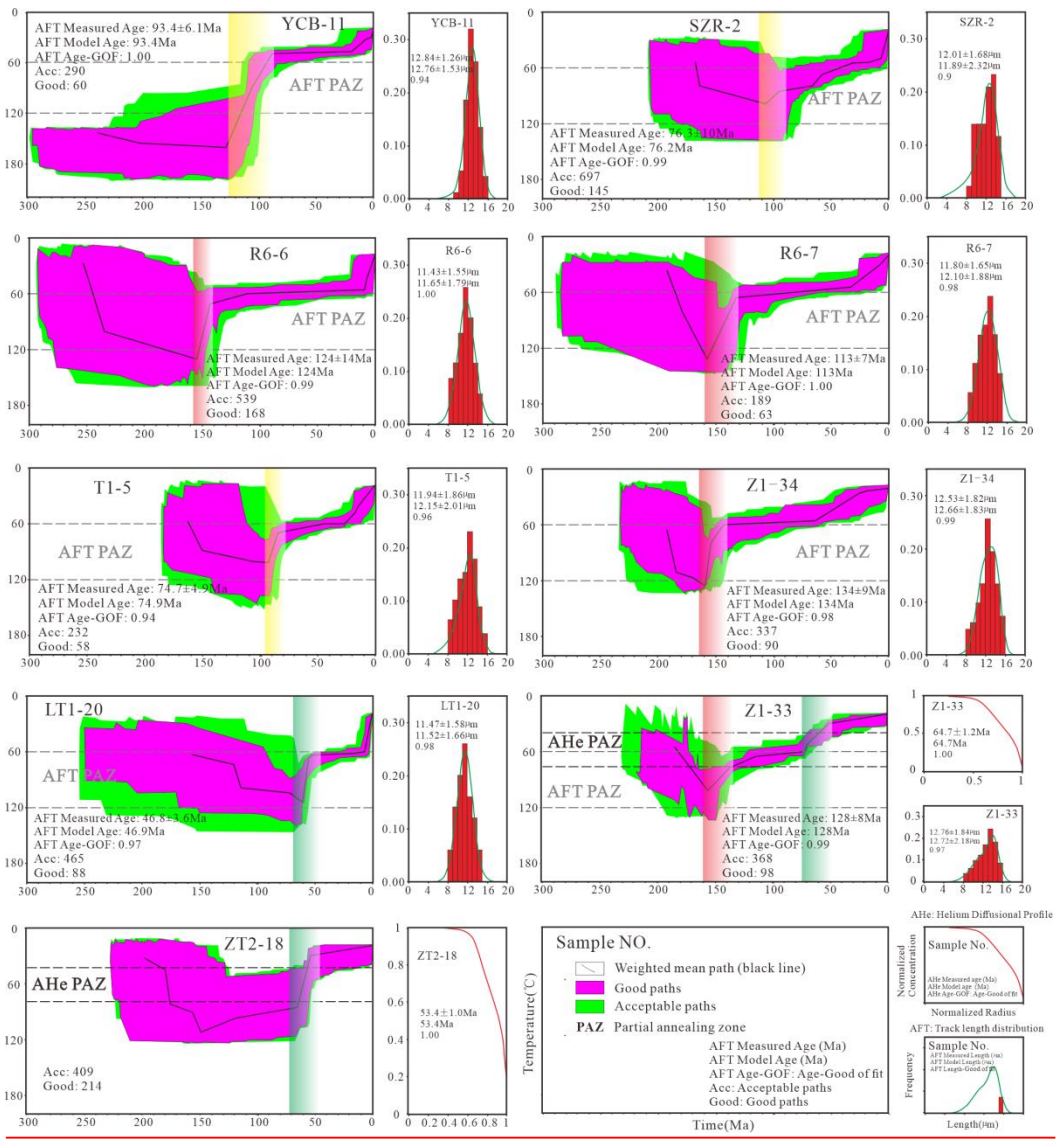

Fig.7 Thermal history inverse modeling calculated by HeFTy (Ketcham, 2005), using the model of Ketcham et al. (2007) and Flowers et al. (2009). HeFTy modeling tests possible t – T curves by using the Monte-Carlo inverse modeling approach. Shaded parts of different colors represent different cooling periods.

5 Discussion

设置格式[残留旳、余温]: 居中, 缩进: 首行缩进: 0 字符

删除[残留旳、余温]:

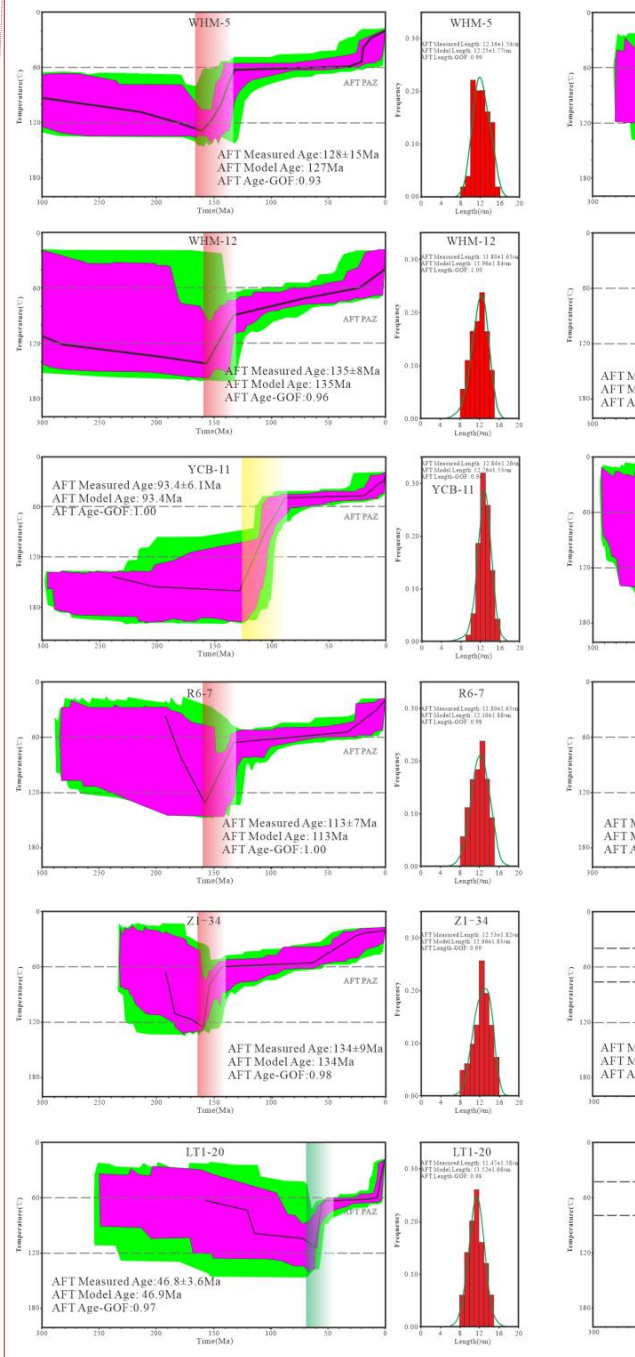

Fig.6 Thermal history inverse modeling calculated by HeFTy (Ketcham, 2005), using the model of Ketcham et al. (2007) and Flowers et al. (2009). HeFTy modeling tests possible t …

设置格式[残留旳、余温]: 字体颜色: 自动设置

From the thermal history simulation paths, the exhumation initiation times generally fall in the late Jurassic; however, there are still differences. The exhumation of the TH region was later, while the other region was earlier, which is related to the tectonic evolution and stress of their respective locations. Additionally, the exhumation intensity varies from east to west across the regions. For example, the samples from the MH region indicate that exhumation occurred earlier in the western samples compared to those in the eastern side. These observations are closely linked to the reverse thrusting and imbrication along the western margin (Fig. 8).

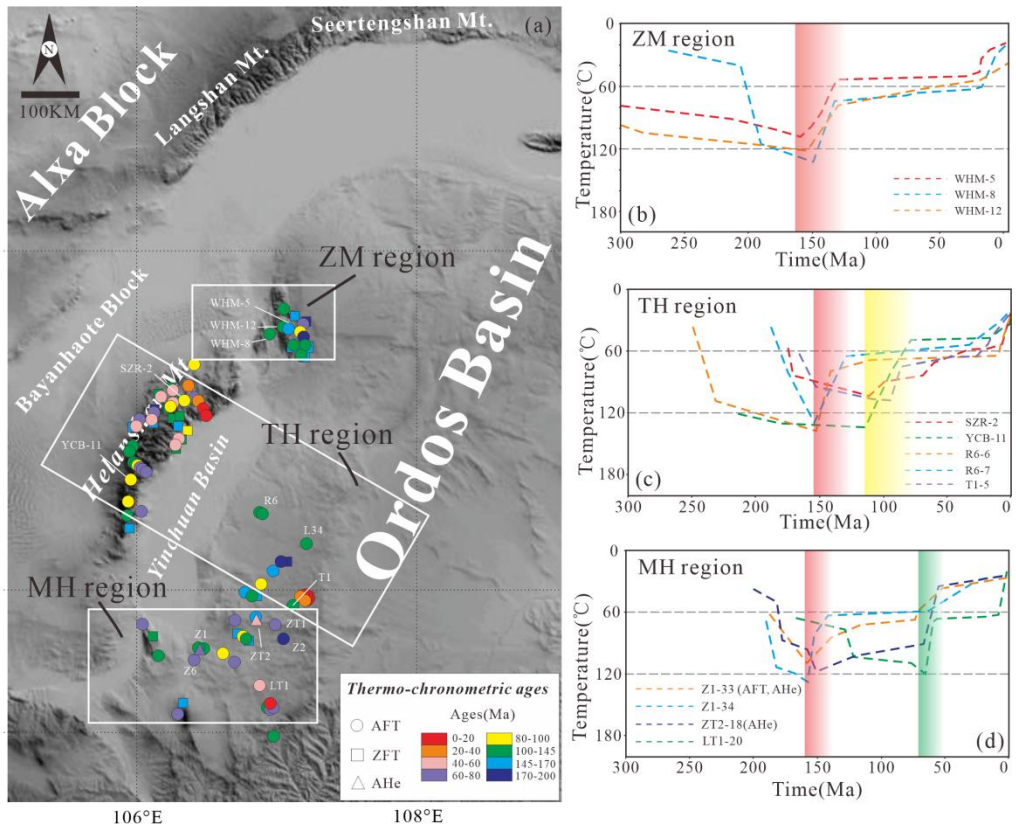

Fig.8 (a) Summary of all available thermochronology data The data sources are the same as in Fig. 2. (b-d), The thermal history paths summarized in this study are from the ZM region, TH region, and MH region, respectively.

删除[残留的、余温]: uplift
设置格式[残留的、余温]: 字体颜色: 自动设置
删除[残留的、余温]: for the three sample sections
删除[残留的、余温]: middle Taole-Hengshanbao part
设置格式[残留的、余温]: 字体颜色: 自动设置
删除[残留的、余温]: uplifted
删除[残留的、余温]: northern and southern parts
删除[残留的、余温]: were uplifted
设置格式[残留的、余温]: 字体颜色: 自动设置
删除[残留的、余温]: uplift
设置格式[残留的、余温]: 字体颜色: 自动设置
删除[残留的、余温]: in the northern part, the uplift rate
设置格式[残留的、余温]: 字体颜色: 自动设置
删除[残留的、余温]: southern part
删除[残留的、余温]: uplift
设置格式[残留的、余温]: 字体颜色: 自动设置
删除[残留的、余温]: 7
设置格式[残留的、余温]: 字体颜色: 自动设置
设置格式[残留的、余温]: 居中, 缩进: 首行缩进: 0 字符
设置格式[残留的、余温]: 字体:(默认)Times New Ro
设置格式[残留的、余温]: 普通(网站), 缩进: 首行缩进
设置格式[残留的、余温]: 字体:(默认)Times New Ro
设置格式[残留的、余温]: 字体:(默认)Times New Ro
设置格式[残留的、余温]: 字体:(默认)Times New Ro
设置格式[残留的、余温]: 字体:(默认)Times New Ro
设置格式[残留的、余温]: 字体:(默认)Times New Ro
设置格式[残留的、余温]: 字体:(默认)Times New Ro
设置格式[残留的、余温]: 字体:(默认)Times New Ro
设置格式[残留的、余温]: 字体:(默认)Times New Ro
设置格式[残留的、余温]: 字体:(默认)Times New Ro
设置格式[残留的、余温]: 字体:(默认)Times New Ro

5.1 Exhumation Process Differences and Geological Responses in the central-northern section of the western margin of the Ordos Basin Constrained by Low-Temperature Thermochronology

5.1.1 The ZM region

Based on the test results, the exhumation rate of this area can be calculated. The calculation formula is:

$$U = (\theta - T_0) / K \times F \quad (1)$$

Here, U represents the exhumation rate (the exhumation rate of apatite since it entered the annealing zone), measured in m/Ma; θ is the closure temperature of the mineral, in ℃; K is the geothermal gradient, in ℃/100m; T_0 is the mean annual surface temperature, in ℃; and F represents the fission-track age, in Ma. For the sake of discussion and comparison, this paper adopts the same parameters as Zhao Hongge (2007), with K set at 4 ℃/100m, T0 at 25 ℃, and θ at 110 ℃.

The author also conducted thermochronology work in the ZM region this year and inverted its exhumation history and thermal history, indicate that the region underwent three major exhumation stages since the Mesozoic: Late Jurassic (160 Ma-150 Ma), this phase marks the first major exhumation stage in the area, with an average exhumation rate of ca. 45 m/Ma and an average cooling rate of ca. 2 ℃/Ma. This exhumation corresponds to the early stages of the Yanshanian orogeny in the region, triggering reverse thrusting and imbrication, as evidenced by the

设置格式[残留的、余温]: 字体颜色: 自动设置
设置格式[残留的、余温]: 字体: 加粗
删除[残留的、余温]: **Uplift**
设置格式[残留的、余温]: 字体颜色: 自动设置
删除[残留的、余温]: **North-Central Western Margin**
删除[残留的、余温]: **Zhuozishan Mt. part**
设置格式[残留的、余温]: 字体: （中文）宋体, 四号
设置格式[残留的、余温]: 缩进: 首行缩进: 9.9 毫米,
设置格式[残留的、余温]: 字体: （中文）宋体, 四号,
设置格式[残留的、余温]: 字体: （中文）宋体, 四号
设置格式[残留的、余温]: 字体颜色: 自动设置
设置格式[残留的、余温]: 字体: （中文）宋体, 四号,
设置格式[残留的、余温]: 缩进: 首行缩进: 11.98 字符
设置格式[残留的、余温]: 字体颜色: 自动设置
设置格式[残留的、余温]: 字体: （中文）宋体, 四号
设置格式[残留的、余温]: 字体: （中文）宋体, 四号,
设置格式[残留的、余温]: 字体: （中文）宋体, 四号
设置格式[残留的、余温]: 字体: （中文）宋体, 四号,
设置格式[残留的、余温]: 字体: （中文）宋体, 四号
设置格式[残留的、余温]: 字体: （中文）宋体, 四号, 下标
设置格式[残留的、余温]: 字体: （中文）宋体, 四号
设置格式[残留的、余温]: 字体: （中文）宋体, 四号
设置格式[残留的、余温]: 字体: （中文）宋体, 四号
设置格式[残留的、余温]: 字体: （中文）宋体, 四号
设置格式[残留的、余温]: 字体颜色: 自动设置
删除[残留的、余温]: The thermal history inversion resul
删除[残留的、余温]: uplift
设置格式[残留的、余温]: 字体颜色: 自动设置
删除[残留的、余温]: after
删除[残留的、余温]:
删除[残留的、余温]:
删除[残留的、余温]: T
删除[残留的、余温]: uplift

inversion results of all three samples; Early Cretaceous - Oligocene (130 Ma - 30 Ma), this stage represents a period of slow cooling, with an average exhumation rate of ca. 10 m/Ma and an average cooling rate of ca. 1℃/Ma, suggesting the absence of significant tectonic events during this time. The timing and exhumation differences among the samples during this phase may reflect the varying effects of different episodes of the Yanshanian orogeny (stages II, III, and IV) on the region; Cenozoic (since ca. 30 Ma), The most recent exhumation stage is associated with the Himalayan orogeny, which caused further significant exhumation in the region, with an average exhumation rate of ca. 30 m/Ma and an average cooling rate of ca. 1.2 ℃/Ma..**5.1.2 The TH region**

In the Taole-Hengshanbao part, two samples from well R6 have peak ages of 161 Ma, 146 Ma, 78 Ma, and 74 Ma, suggesting possible tectonic events during the Late Jurassic and Late Cretaceous. The thermal history models of both samples show similar results, indicating three phases of exhumation: Late Jurassic (155 Ma-145 Ma), a period of significant exhumation begins, with an average exhumation rate of ca. 48 m/Ma and an average cooling rate of ca. 2.4 ℃/Ma; Early Cretaceous - Oligocene (145 Ma-30 Ma), this phase is characterized by slow exhumation, with an average exhumation rate of ca. 7.5 m/Ma and an average cooling rate of ca. 0.3 ℃/Ma; Cenozoic (ca. 30 Ma-present), a period of intense and rapid exhumation occurs, with an average exhumation rate of ca. 25

删除[残留的、余温]: . Stratigraphically, the Late Jurassi
设置格式[残留的、余温]: 字体:（默认）Times New Ro
设置格式[残留的、余温]: 字体颜色: 自动设置
删除[残留的、余温]: T
设置格式[残留的、余温]: 字体颜色: 自动设置
删除[残留的、余温]: uplift
设置格式[残留的、余温]: 字体颜色: 自动设置
删除[残留的、余温]: uplift
设置格式[残留的、余温]: 字体颜色: 自动设置
删除[残留的、余温]: uplift
设置格式[残留的、余温]: 字体颜色: 自动设置
设置格式[残留的、余温]: 字体颜色: 自动设置
删除[残留的、余温]:
设置格式[残留的、余温]: 字体:（默认）Times New Ro
设置格式[残留的、余温]: 字体颜色: 自动设置
删除[残留的、余温]: **Taole-Hengshanbao part**
删除[残留的、余温]: uplift
设置格式[残留的、余温]: 字体颜色: 自动设置
删除[残留的、余温]: uplift
设置格式[残留的、余温]: 字体颜色: 自动设置
设置格式[残留的、余温]: 字体颜色: 自动设置
删除[残留的、余温]: uplift
设置格式[残留的、余温]: 字体颜色: 自动设置
设置格式[残留的、余温]: 字体颜色: 自动设置
删除[残留的、余温]: uplift
设置格式[残留的、余温]: 字体颜色: 自动设置
设置格式[残留的、余温]: 字体颜色: 自动设置

m/Ma and an average cooling rate of ca. 1 ℃/Ma. The ages recorded in samples R6-6 and R6-7 are basically the same. The slight differences in their AFT model results arise because R6-6 was located deeper, meaning it exited the partial annealing zone later than R6-7 during exhumation. This caused the AFT age constraints for R6-6 to be slightly younger. For the T1-5 sample, located in the THD, exhumation began at the end of the Early Cretaceous, with an average exhumation rate of ca. 50 m/Ma and an average cooling rate of ca. 2 ℃/Ma. This area previously had a complete sedimentary sequence and extensive sediment distribution, forming the thick Tianhuan syncline in the Ordos Basin (Zhao et al., 2007a).。

The exhumation in this area is related to the exhumation in the neighboring Helanshan Mountain region and the intense faulting and subsidence in the Yinchuan Graben. The thermal history models of the two Helanshan Mountain samples (SZR-2 and YCB-11) also have a certain pattern in spatial and temporal distribution: The YCB-11 sample in the south entered a rapid cooling stage from the end of the Early Cretaceous to the Late Cretaceous (130 Ma-95 Ma), with an average exhumation rate of ca. 46 m/Ma and an average cooling rate of ca. 1.8 ℃/Ma, followed by slow cooling with an average exhumation rate of ca. 2.5 m/Ma until the Eocene (~35 Ma), after which it rapidly exhumation to the surface, with an average exhumation rate of ca. 18 m/Ma and an average cooling rate of ca. 0.7 ℃/Ma. The northern SZR-2 sample, however,

删除[残留的、余温]: consistent within the error range

删除[残留的、余温]: uplift

设置格式[残留的、余温]: 字体颜色: 自动设置

设置格式[残留的、余温]: 字体颜色: 自动设置

设置格式[残留的、余温]: 字体颜色: 自动设置

设置格式[残留的、余温]: 字体颜色: 自动设置

删除[残留的、余温]: uplift

设置格式[残留的、余温]: 字体颜色: 自动设置

删除[残留的、余温]: part

设置格式[残留的、余温]: 字体颜色: 自动设置

删除[残留的、余温]: uplift

设置格式[残留的、余温]: 字体颜色: 自动设置

删除[残留的、余温]: show a spatial pattern

设置格式[残留的、余温]: 字体颜色: 自动设置

删除[残留的、余温]: the southern YCB-11 sample experienced rapid cooling at the end of the Early Cretaceous (130 Ma-95 Ma),

设置格式[残留的、余温]: 字体颜色: 自动设置

删除[残留的、余温]: uplifted

设置格式[残留的、余温]: 字体颜色: 自动设置

设置格式[残留的、余温]: 字体颜色: 自动设置

shows a delayed cooling history at essentially the same rate of exhumation, with cooling events occurring primarily after the Early Cretaceous. The exhumation pattern, with earlier exhumation in the south and later exhumation in the north, aligns with previous studies on the Helanshan Mountain region (Ma et al., 2019).

5.1.3 The MH region

In the southern, Majiatan-Huianbao part, two samples from well Z1 (Z1-33 and Z1-34) indicate that exhumation in the well began during the Late Jurassic (ca. 160 Ma). Combined AFT and AHe inversion results show that sample Z1-33 experienced rapid exhumation between 158 Ma and 137 Ma, with an average exhumation rate of ca. 45 m/Ma and an average cooling rate of ca. 1.8 ℃/Ma, followed by slower exhumation from 137 Ma to 110 Ma, with an average exhumation rate of ca. 13 m/Ma and an average cooling rate of ca. 0.52 ℃/Ma, and then entered another phase of intense exhumation between 70 Ma and 50 Ma, with an average exhumation rate of ca. 37.5 m/Ma and an average cooling rate of ca. 1.5 ℃/Ma. Sample Z1-34, constrained only by AFT data, shows large-scale exhumation starting from 160 Ma to 140 Ma, a slow exhumation phase from 140 Ma to 64 Ma, and then a rapid exhumation event. Since the temperature at 64 Ma is beyond the AFT-sensitive temperature range, the thermal history model of well Z1, especially for the later stages of exhumation and cooling, is more reliably constrained

设置格式[残留的、余温]: 字体颜色: 自动设置
删除[残留的、余温]: uplift
设置格式[残留的、余温]: 字体颜色: 自动设置
删除[残留的、余温]: uplift
设置格式[残留的、余温]: 字体颜色: 自动设置
删除[残留的、余温]: uplift
设置格式[残留的、余温]: 字体颜色: 自动设置
删除[残留的、余温]: 2
删除[残留的、余温]: Majiatan-Huianbao part
删除[残留的、余温]: uplift
设置格式[残留的、余温]: 字体颜色: 自动设置
删除[残留的、余温]: uplift
设置格式[残留的、余温]: 字体颜色: 自动设置
设置格式[残留的、余温]: 字体颜色: 自动设置
删除[残留的、余温]: uplift
设置格式[残留的、余温]: 字体颜色: 自动设置
设置格式[残留的、余温]: 字体颜色: 自动设置
删除[残留的、余温]: uplift
设置格式[残留的、余温]: 字体颜色: 自动设置
删除[残留的、余温]: uplift
设置格式[残留的、余温]: 字体颜色: 自动设置
删除[残留的、余温]: uplift
设置格式[残留的、余温]: 字体颜色: 自动设置

by the dual-dating sample Z1-33. The AFT simulation of sample LT1-20 reveals an exhumation event between 60 Ma and 55 Ma, with an average exhumation rate of ca. 60 m/Ma and an average cooling rate of ca. 4 ℃ /Ma, and the AHe thermal history simulation of sample ZT2-18 similarly shows an exhumation event from 62 Ma to 52 Ma, with an average exhumation rate of ca. 65 m/Ma and an average cooling rate of ca. 6.5 ℃ /Ma. This indicates an early Cenozoic tectonic cooling event in the region.

删除[残留旳、余温]: uplift

设置格式[残留旳、余温]: 字体颜色: 自动设置

设置格式[残留旳、余温]: 字体颜色: 自动设置

删除[残留旳、余温]: uplift

设置格式[残留旳、余温]: 字体颜色: 自动设置

设置格式[残留旳、余温]: 字体颜色: 自动设置

删除[残留旳、余温]: For the T1-5 sample, located in the Tianhuan syncline, uplift began at the end of the Early Cretaceous. This area previously had a complete sedimentary sequence and extensive sediment distribution, forming the thick Tianhuan syncline in the Ordos Basin (Zhao et al., 2007a).。

5.2 Transformation of the Meso-Cenozoic Tectonic Regime and Regional Dynamic Background in the North-Central Western Margin

At the end of the Paleoproterozoic, the Ordos Block formed and merged with the North China Craton. Following this, under an extensional tectonic environment, large-scale rifting occurred, creating northeast-trending rift troughs with some structural inheritance from the basement, which was covered by strata from different periods, including strata of the Proterozoic, Paleozoic, Mesozoic, and Cenozoic eras (Bao et al., 2019; Zhao et al., 2019). In the early Palaeozoic, the Ordos region transitioned into a stable cratonic basin. During multiple marine transgressions and regressions, a set of widespread marine carbonate sediments, interbedded with clastic rocks, was deposited across the region. The large-scale Caledonian orogeny caused a depositional hiatus between

删除[残留旳、余温]: .

删除[残留旳、余温]: These troughs were subsequently covered by stratigraphic deposits from different periods

删除[残留旳、余温]: Early

删除[残留旳、余温]: Paleozoic

删除[残留旳、余温]: the

Ordovician and Carboniferous strata, resulting in an unconformable contact between the two. Since the late Palaeozoic, the Ordos Basin has begun the transition from sea-land intersection to terrestrial sedimentation, and the development of the North China marginal sea - coastal shallow sea sedimentary. During the Late Triassic to Early Cretaceous, the basin saw intracratonic fluvial-lacustrine sedimentation. Since the Late Cretaceous, the basin has entered a phase of overall exhumation and peripheral subsidence. From the late Mesozoic, the Ordos Basin became an independent sedimentary basin. Its sedimentary evolution has been primarily influenced by the Mesozoic-Cenozoic tectonic systems, undergoing multiple sedimentary cycles and exhumation-related transformations (Fig. 9).

In the Triassic period, influenced by the Indosinian Orogeny, the Qinling-Qilian ancient ocean basin finally closed. The mountains collided and continued to compress, resulting in sedimentary hiatuses or erosion. Therefore, the Late Triassic and Early Jurassic strata were in parallel unconformable contact (Zhang et al., 2001). The Indosinian tectonic stress originated from the collision and docking of the South China Plate and the North China Plate during the Triassic period, resulting in a north-south stress field (Peng, et al., 2024).

The Yanshanian orogeny was the primary tectonic deformation period for the Ordos Basin, with the particularly intense compression

删除[残留旳、余温]: systems

删除[残留旳、余温]: L

删除[残留旳、余温]: Paleozoic

删除[残留旳、余温]: the Ordos Basin has transitioned from marine to terrestrial facies deposition, evolving from a coastal-continental margin to shallow marine sediments, dominated by swamp, deltaic, and fluvial deposits

设置格式[残留旳、余温]: 字体颜色: 自动设置

删除[残留旳、余温]: the basin has experienced overall uplift and surrounding faulting.

删除[残留旳、余温]: L

删除[残留旳、余温]: uplift

设置格式[残留旳、余温]: 字体颜色: 自动设置

设置格式[残留旳、余温]: 字体颜色: 自动设置

删除[残留旳、余温]: 8

设置格式[残留旳、余温]: 字体颜色: 自动设置

设置格式[残留旳、余温]: 字体颜色: 自动设置

deformation and exhumation erosion in the Late Jurassic. These movements caused the Jurassic and underlying sedimentary layers to become involved in widespread deformation, resulting in a clear angular unconformity with the overlying strata. This deformation was especially pronounced along the western margin of the basin, where much of the surface deformation that is observed today had already taken shape during this period (Darby et al., 2002). The tectonic stress of the Yanshanian orogeny originated from the Tethys tectonic domain, eastward compression of the Alxa block, westward subduction of the Pacific plate, and closure of the Okhotsk Ocean.

设置格式[残留旳、余温]: 字体颜色: 自动设置

删除[残留旳、余温]: with the Late Jurassic tectonic movements being particularly intense

删除[残留旳、余温]: In the Early Cretaceous, the deep thermal material in the basin began to upwell, and the upper crust entered a tensional tectonic environment. Since the Late Cretaceous, the Ordos Basin has experienced significant uplift and erosion, a process that has continued to the present day (Ren et al., 2007, 2008, 2014, 2017, 2020, 2022).

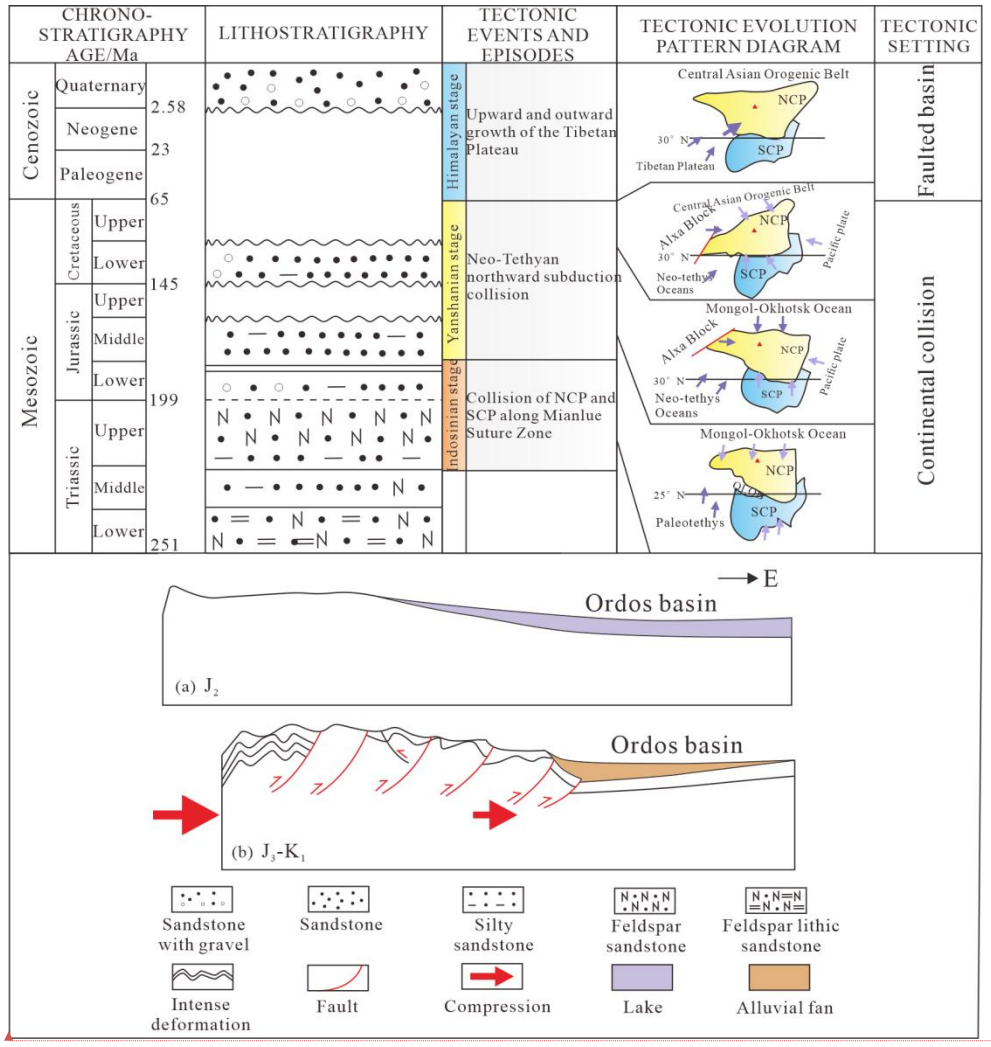

Fig.9 Dynamic model diagram of the northern part of the western margin of Ordos Basin.(Modified from Ma, 2019; Zhang et al., 2021; Peng et al., 2022)

In the Late Jurassic, the Yanshanian orogeny triggered the first major large-scale exhumation in the study area. During this period, the compressional forces that were primarily north-south oriented during the earlier Indosinian orogeny transitioned to an east-west orientation characteristic of the Yanshanian phase (Dong et al., 2007, 2008, 2015; Zhang et al., 2008). This tectonic exhumation event aligns with the peak ages obtained from fission-track at 170 Ma, 161 Ma, and 153 Ma. The tectonic evolution of this phase was controlled by several factors, notably the southwest Tethys tectonic domain, eastward compression from the

设置格式[残留旳、余温]: 字体颜色: 自动设置

删除[残留旳、余温]: 8

设置格式[残留旳、余温]: 字体颜色: 自动设置

删除[残留旳、余温]: During the Triassic period, the Indosinian Orogeny significantly impacted the region, leading to the final closure of the ancient Qinling-Qilian Ocean Basin. The continuous collision and compression of mountain ranges caused uplift and sedimentary hiatuses. As a result, the Late Triassic and Early Jurassic strata exhibit a parallel unconformity (Zhang et al., 2001).

删除[残留旳、余温]: uplift

设置格式[残留旳、余温]: 字体颜色: 自动设置

删除[残留旳、余温]: uplift

设置格式[残留旳、余温]: 字体颜色: 自动设置

删除[残留旳、余温]:

设置格式[残留旳、余温]: 字体颜色: 自动设置

删除[残留旳、余温]: s

Alxa Block, and the closure of the Okhotsk Ocean in the north during the Late Jurassic (Zhao et al., 2023). Additionally, far-field effects from the subduction of the Pacific Plate played a role (Darby et al., 2002, 2007; Faure et al., 2012; Liu et al., 1998; Yang et al., 2008; Zhang et al., 2020, 2021, 2022; Zhao et al., 2023). Previous paleomagnetic studies revealed that the Ordos Basin was undergoing a counterclockwise rotation during this period (Ma et al., 1993; Yang et al., 1990; Zhang et al., 2000). These regional tectonic processes collectively shaped the large-scale exhumation and deformation seen during this period, marking a significant phase in the area's geological history. The comprehensive analysis of stress fields in the Late Jurassic indicates that multiple tectonic blocks around the Ordos Basin experienced subduction, collision, compression, and even mutual rotation. These interactions led to the folding and exhumation of Jurassic strata, accompanied by a series of imbricate thrust faults pushing from west to east (Zhao et al., 1987; Ma et al., 2019; Zhang et al., 2021, 2022). In the ZM region, the collision with the Alxa Block initiated significant exhumation, while in the MH region, the overall exhumation of the Qilian Mountains and its thrusting into the basin resulted in strong thrusting structures. This contributed to the earlier onset of exhumation in areas like ZM region and MH region. The compressional deformation shows a general pattern of stronger exhumation and deformation in the west and at the margins, with weaker

删除[残留的、余温]: 9
删除[残留的、余温]: uplift
设置格式[残留的、余温]: 字体颜色: 自动设置
删除[残留的、余温]: uplift
设置格式[残留的、余温]: 字体颜色: 自动设置
删除[残留的、余温]: northern section
删除[残留的、余温]: uplift
设置格式[残留的、余温]: 字体颜色: 自动设置
删除[残留的、余温]: southern part
删除[残留的、余温]: uplift
设置格式[残留的、余温]: 字体颜色: 自动设置
删除[残留的、余温]: uplift
设置格式[残留的、余温]: 字体颜色: 自动设置
删除[残留的、余温]: Zhuozishan Mt.
删除[残留的、余温]: the Majiatan-Huianbao
删除[残留的、余温]: s
删除[残留的、余温]: uplift
设置格式[残留的、余温]: 字体颜色: 自动设置

effects in the interior of the basin.

The Early Cretaceous was a crucial period in the evolution of the Ordos Basin, the deep thermal material in the basin began to upwell. Northern China was under an extensional tectonic regime, linked to the broader lithospheric thinning and basin development of the North China Craton during this time (Ren et al., 2007, 2008, 2014, 2017, 2020, 2022). In the central Taole region, extensional faults from this period are observable in seismic profiles (Zhao et al., 2007a). Towards the end of the Early Cretaceous, the regional tectonic stress field reversed due to the multiple phases of the Yanshanian orogeny (phases II, III, IV). The area was simultaneously influenced by the northward collision of the Yangtze Plate and the far-field effects of the Pacific Plate. The northern region was affected by the closure of the Okhotsk Ocean, and the western region continued to experience direct compression from the eastward movement of the Alxa Block (Yang et al., 2008; Zhang et al., 2020, 2022; Zhao et al., 2023). The previously deposited strata experienced intensified folding and exhumation under compressional stress. This led to the formation of large-scale south-north-oriented thrust faults and imbricate thrust structures. At this point, the tectonic landscape of the study area is basically formed.During the Cenozoic, the tectonic deformation of the Ordos Basin was primarily driven by the collision between the Indian and Eurasian plates. This is the primary cause of the closure of the Tethys

删除[残留旳、余温]: the Early Cretaceous

删除[残留旳、余温]: 2020

删除[残留旳、余温]: uplift

设置格式[残留旳、余温]: 字体颜色: 自动设置

删除[残留旳、余温]: , resulting in significant structural deformation

删除[残留旳、余温]: By this time, the region’s major tectonic framework had largely formed, and subsequent tectonic movements primarily modified this existing structure.

删除[残留旳、余温]: ,

Ocean and one of the responsible for the stresses applied in the region, with significant tectonic activity occurring during the Eocene to Miocene. The continued Himalayan orogeny caused strong tectonic movements in the region, leading to further exhumation of the strata. The strata predominantly displaying parallel and angular unconformities. This tectonic activity has significantly shaped the present-day landscape. The neighboring Alxa region, located at the northeastern edge of the Tibetan Plateau, was affected by the plateau's Cenozoic exhumation. Its deformation is closely linked to the evolution of the Tibetan Plateau (Zhang et al., 2023; Rao et al., 2016; Lei et al., 2022). Concurrently, the Pacific Plate continued its northwestward subduction during this period. Numerous geochronological records document the exhumation and northeastward expansion of the northeastern Tibetan Plateau during the Cenozoic, particularly in the Eocene and Miocene (England and Housemann, 1986; Tapponnier et al., 2001; Wang et al., 2008; Lease et al., 2011, 2012; Craddock et al., 2011; Ding et al., 2022; Peng et al., 2019; Zhao et al., 2023; Chen et al., 2024; Zhang et al., 2020). Low-temperature thermochronology data, along with thermal history reconstructions constrained by AHe and AFT, reveal rapid exhumation during the Eocene to Miocene, likely a result of the far-field effects of the Cenozoic exhumation of the northeastern Tibetan Plateau and the northwestward subduction of the Pacific Plate.

删除[残留旳、余温]: uplift
设置格式[残留旳、余温]: 字体颜色: 自动设置
删除[残留旳、余温]: mountains
删除[残留旳、余温]: ,
删除[残留旳、余温]: with the
删除[残留旳、余温]: uplift
设置格式[残留旳、余温]: 字体颜色: 自动设置
删除[残留旳、余温]: uplift
设置格式[残留旳、余温]: 字体颜色: 自动设置
删除[残留旳、余温]: uplift
设置格式[残留旳、余温]: 字体颜色: 自动设置
删除[残留旳、余温]: uplift
设置格式[残留旳、余温]: 字体颜色: 自动设置

Overall, the study area has undergone the Indosinian, Yanshanian, and Himalayan orogenies since the Mesozoic era. In the central-northern section of the western margin of the basin, especially during the Yanshanian period, the Alxa rigid block sandwiched between the South China and North China plates is squeezed out in a southeast direction, directly affecting the Helanshan Mountains and the northern part of the western margin of the basin, causing the stress direction to shift towards a nearly east-west direction.

6 Conclusion

(1) This study used apatite fission-track (AFT) and apatite (U-Th)/He (AHe) dating methods, combined with thermal history modeling, to precisely constrain the exhumation and cooling history of the central-northern sections of the western margin of the Ordos Basin. The analysis reveals significant differences in the timing and intensity of exhumation across different regions: ZM region experienced a large-scale exhumation during the Late Jurassic (160-150 Ma), slow exhumation at Early Cretaceous - Oligocene (130 Ma-30 Ma), and severe exhumation after Oligocene (30 Ma-); TH region began at Late Jurassic - Early Cretaceous (155 Ma-145 Ma), slowly exhumation at Early Cretaceous - Oligocene (145 Ma-30 Ma), and then violently exhumation; MH region experienced a significant exhumation at Late Jurassic - Early Cretaceous (158 Ma-137 Ma), with a slightly slower exhumation rate at 137 Ma-110

删除[残留的、余温]: ys
删除[残留的、余温]: The Indosinian tectonic stress
删除[残留的、余温]: part
删除[残留的、余温]: The direction of the tectonic stress
设置格式[残留的、余温]: 缩进: 首行缩进: 0 字符, 无
设置格式[残留的、余温]: 字体颜色: 自动设置
删除[残留的、余温]: utilizes
设置格式[残留的、余温]: 字体:（默认）Times New Ro
删除[残留的、余温]: Apatite Fission Track
设置格式[残留的、余温]: 字体颜色: 自动设置
删除[残留的、余温]: Apatite
删除[残留的、余温]: and existing geological evidence
删除[残留的、余温]: uplift
设置格式[残留的、余温]: 字体颜色: 自动设置
删除[残留的、余温]: central and northern
删除[残留的、余温]: uplift
设置格式[残留的、余温]: 字体颜色: 自动设置
设置格式[残留的、余温]: 字体颜色: 自动设置
删除[残留的、余温]: Zhuozishan part
删除[残留的、余温]: uplift
设置格式[残留的、余温]: 字体颜色: 自动设置
设置格式[残留的、余温]: 字体颜色: 自动设置
设置格式[残留的、余温]: 字体颜色: 自动设置
删除[残留的、余温]: followed by slow uplift between
删除[残留的、余温]: Taole-Hengshanbao part
删除[残留的、余温]: uplifting
设置格式[残留的、余温]: 字体颜色: 自动设置
设置格式[残留的、余温]: 字体颜色: 自动设置
删除[残留的、余温]: around 155-145 Ma, followed by a
删除[残留的、余温]: Majiatan-Huianbao part
删除[残留的、余温]: uplift
设置格式[残留的、余温]: 字体颜色: 自动设置
设置格式[残留的、余温]: 字体颜色: 自动设置

Ma, and entered a severe exhumation stage again at Late Cretaceous - Eocene (70 Ma-50 Ma). Overall, the northern and southern sections began earlier, while the central section initiated exhumation slightly later. These findings highlight the spatial variation in exhumation timing and rates within the western Ordos Basin.

(2) The study reveals that the Yanshanian orogeny had the most significant tectonic impact on the study area. Multiple exhumation events during the Mesozoic are responses to the multi-phase Yanshanian orogeny in this region. Since the Cenozoic, rapid exhumation influenced by the Himalayan orogeny has shaped the current landscape.

Competing interests

The contact author has declared that none of the authors has any competing interests.

Acknowledgements

Financial support for this study were jointly provided by the Major Projects of Changqing Oilfield Company (ZDZX2021). Our heartfelt gratitude is given to those anonymous reviewers for their scientific and linguistic revisions to the manuscript.

Conferences

[1] Bao Hongping, Shao Dongbo, Hao Songli, et al. Basement Structure and Early Sedimentary Cover Evolution of the Ordos Basin[J]. Earth Science Frontiers, 2019, 26(1): 33-43.

[2] Barbarand J, Carter A, Wood I, et al. Compositional and structural control of fission-track annealing in apatite[J]. Chemical Geology, 2003, 198(1-2): 107-137.

[3] Carlson W D, Donelick R A, Ketcham R A. Variability of apatite fission-track

设置格式[残留的、余温]: 字体颜色: 自动设置

删除[残留的、余温]: between 158-137 Ma, with a slower uplift phase from 137-110 Ma, and a period of rapid uplift again between 70-50 Ma.

删除[残留的、余温]: uplifting

删除[残留的、余温]: middle

删除[残留的、余温]: uplift

设置格式[残留的、余温]: 字体颜色: 自动设置

删除[残留的、余温]: uplift

设置格式[残留的、余温]: 字体颜色: 自动设置

设置格式[残留的、余温]: 缩进: 首行缩进: 0 字符

删除[残留的、余温]: （2）This study effectively reveals the uplift movements of the northern section of the western margin during the Mesozoic and Cenozoic using low-temperature thermochronology method. It suggests

设置格式[残留的、余温]: 字体:（默认）Times New Roman, （中文）宋体, 四号, 字体颜色: 自动设置

设置格式[残留的、余温]: 字体颜色: 自动设置

删除[残留的、余温]: uplift

设置格式[残留的、余温]: 字体颜色: 自动设置

删除[残留的、余温]: uplift

设置格式[残留的、余温]: 字体颜色: 自动设置

annealing kinetics: I. Experimental results[J]. American mineralogist, 1999, 84(9): 1213-1223.
[4] Chen G M, Qin H T, Huang X F, et al. Cenozoic tectonic evolution of the Liupan Shan area: Evidence from zircon and apatite fission tracks[J]. Chinese Journal of Geophysics, 2024, 67(3): 1147-1168.
[5] Chen Gang, Wang Zhiwei, Bai Guojun, Sun Jianbo, Zhang Huiruo, Li Xiangdong. Peak Age Events and Their Sedimentary-Tectonic Responses in the Mesozoic-Cenozoic Ordos Basin[J]. Geology in China, 2007(03): 375-383.
[6] Chen Gang. Composition of Mesozoic Terrigenous Clastic Rocks and Their Tectonic Attributes in the Ordos Basin[J]. Acta Sedimentologica Sinica, 1999(03): 409-413.
[7] Craddock W, Kirby E, Zhang H P. 2011. Late Miocene-Pliocenerange growth in the interior of the northeastern TibetanPlateau, Lithosphere,3(6):420-438.
[8] Darby B J, Ritts B D. Mesozoic contractional deformation in the middle of the Asian tectonic collage: the intraplate Western Ordos fold–thrust belt, China[J]. Earth and Planetary Science Letters, 2002, 205(1-2): 13-24.
[9] Darby B J, Ritts B D. Mesozoic structural architecture of the Lang Shan, North-Central China: Intraplate contraction, extension, and synorogenic sedimentation[J]. Journal of Structural Geology, 2007, 29(12): 2006-2016.
[10] Ding L, Kapp P, Cai F, et al. Timing and mechanisms of Tibetan Plateau uplift[J]. Nature Reviews Earth & Environment, 2022, 3(10): 652-667.
[11] Dong Shuwen, Zhang Yueqiao, Chen Xuanhua, et al. Formation and Deformation Characteristics of the Late Jurassic Multidirectional Convergent Tectonic System in East Asia[J]. Acta Geoscientia Sinica, 2008, 29(3): 306-317.
[12] Dong Shuwen, Zhang Yueqiao, Li Hailong, et al. The "Yanshan Movement" and the Late Mesozoic Multiplate Convergence Tectonics in East Asia: Commemorating the 90th Anniversary of the "Yanshan Movement"[J]. Science in China: Earth Sciences, 2019, 49(6): 913-938.
[13] Dong Shuwen, Zhang Yueqiao, Long Changxing, et al. New Interpretations of the Jurassic Tectonic Transformations and the Yanshan Movement in China[J]. Acta Geologica Sinica, 2007, 81(11): 1449-1461.
[14] Dong Yunpeng, Li Wei, Zhang Feifei, et al. Formation and Evolution of the Helan Mountain in the Northern Section of the North-South Tectonic Belt[J]. Journal of Northwest University (Natural Science Edition), 2021, 51(6): 951-968
[15] England P, Houseman G, 1986. Finite strain calculations of continentaldeformation:2.Comparison with the India-Asia Collision Zone.Journalof Geophysical Research:Solid Earth,9l(B3):3664-3676.
[16] Farley K A, Wolf R A, Silver L T. The effects of long alpha-stopping distances on (U-Th)/He ages[J]. Geochimica et cosmochimica acta, 1996, 60(21): 4223-4229.
[17] Faure M, Lin W, Chen Y. Is the Jurassic (Yanshanian) intraplate tectonics of North China due to westward indentation of the North China block?[J]. Terra Nova, 2012, 24(6): 456-466.
[18] Flowers R M, Farley K A, Ketcham R A. A reporting protocol for thermochronologic modeling illustrated with data from the Grand Canyon[J]. Earth

and Planetary Science Letters, 2015, 432: 425-435.
[19] Gallagher K. Transdimensional inverse thermal history modeling for quantitative thermochronology[J]. Journal of Geophysical Research: Solid Earth, 2012, 117(B2).
[20] Gan Kewen. On the Genesis Mechanism of Thrust Belts and Hydrocarbon Prospects of the Western Margin of the Ordos Basin[J]. In: Yang Junjie. Thrust Tectonics and Hydrocarbon in the Western Ordos Basin. Lanzhou: Gansu Science and Technology Press, 1990, 31239.
[21] Gao Feng, Wang Yuejun, Liu Shunsheng, Hu Baoqing. Study on the Thermal History of the Western Margin of the Ordos Basin Using Apatite Fission Track Analysis[J]. Geotectonica et Metallogenia, 2000(01): 87-91.
[22] Gao Shaohua. Mesozoic-Cenozoic Evolutionary Modification of the Lateral Structural Belt in the Central Western Ordos Basin and Its Significance for Oil and Gas[D]. Xi'an: Northwest University, 2014.
[23] Gleadow A J W, Seiler C, Rink W J, et al. Fission track dating and thermochronology[J]. Encyclopedia of scientific dating Methods, 2015: 285-296.
[24] Hasebe N, Barbarand J, Jarvis K, et al. Apatite fission-track chronometry using laser ablation ICP-MS[J]. Chemical Geology, 2004, 207(3-4): 135-145.
[25] He Dengfa, Sun Fangyuan, Zhai Yonghe, et al. Formation Evolution of the Shigouyi Anticline in the Western Ordos Basin and Its Tight Sandstone Gas Accumulation Model[J]. Oil & Gas Geology, 2021, 42(2): 370-390.
[26] Jiang Suyang, Huang Wenhui, Zhang Yongsheng, et al. Tectonic Setting and Provenance Analysis of the Sandstones from the Sandaokan Formation in the Northern Segment of the Western Ordos Basin[J]. Journal of Northeast Petroleum University, 2019, 43(4): 17-28.
[27] Ketcham R A, Carter A, Donelick R A, et al. Improved modeling of fission-track annealing in apatite[J]. American Mineralogist, 2007, 92(5-6): 799-810.
[28] Ketcham R A. Forward and inverse modeling of low-temperature thermochronometry data[J]. Reviews in mineralogy and geochemistry, 2005, 58(1): 275-314.
[29] Lease R O,Burbank D W, Hough B, et al. 2012. Pulsed Miocenerange growth in northeastern Tibet: insights from XunhuaBasin magnetostratigraphy and provenance. GSA Bull.,124(5-6):657-677.
[30] Lease R.O., Burbank D W, Clark M K, et al. 2011. Middle Miocenereorganization of deformation along the northeastern TibetanPlateau, Geology,39(4):359-362.
[31] Lei Q, Yu J, Zhang P, et al. Tectonic geomorphology and prehistoric earthquakes of the West Helanshan fault, West Ordos, and its implications for regional tectonics and seismic hazard[J]. Tectonophysics, 2022, 833: 229375.
[32] Li Bin. Study on the Thrust Belt Structure and Hydrocarbon Controlling Factors in the Western Ordos Basin[D]. Northwest University, 2019.
[33] Li Bin. Tectonic Characteristics and Hydrocarbon Accumulation Studies of the Foreland Basin in the Western Ordos Basin[D]. Graduate School of the Chinese Academy of Sciences (Guangzhou Institute of Geochemistry), 2006.
[34] Li Tianbin. Characteristics and Evolution of Thrust Structures in the Western

Ordos Basin[D]. China University of Geosciences (Beijing), 2006.
[35] Liu Chiyang, Zhao Hongge, Wang Feng, et al. Mesozoic Tectonic Characteristics of the Western Margin of the Ordos Basin[J]. Acta Geologica Sinica, 2005, 79(6): 737-747.
[36] Liu Hefu. Types of Foreland Basins and Styles of Fold-Thrust Structures[J]. Earth Science Frontiers, 1995, 2(3): 59-68.
[37] Liu Jianhui. Cenozoic Extensional Uplift of the Helan Mountains and Qinling Mountains and Analysis of Fault Frictional Heating Using Apatite Fission Track Method[J]. International Seismological Dynamics, 2010, 31(3): 31-33.
[38] Liu S F, The coupling mechanism of basin and orogen in the western ordos Basin and adjacent regionsof China[]. Journal of Asian Eart h Science,1998,16(4):369-383.
[39] Liu Shaofeng, Yang Shigong. North-South Differences and Their Formation Mechanism on the Western Margin of the Ordos Basin[J]. Geological Science, 1997, 32(3): 397-408.
[40] Ma Jinghui, He Dengfa. Mesozoic-Cenozoic Tectonic Events in the Helan Mountain Tectonic Belt and Adjacent Areas: Constraints from Unconformities and Fission Track Analysis[J]. Acta Petrologica Sinica, 2019, 35(4): 1121-1142.
[41] Ma X.H., Xing L.S., Yang Z.Y., et al. Paleomagnetic Study of the Ordos Basin since the Late Paleozoic [J]. Chinese Journal of Geophysics, 1993, (01): 68-79.
[42] Ouyang Zhengjian, Chen Hongde, Feng Juanping. Tectonic Characteristics and Evolution of the Central and Southern Segments of the Western Margin of the Ordos Basin[J]. Modern Geology, 2012, 26(04): 691-695.
[43] Peng H , Wang J , Liu C ,et al.Thermochronological constraints on the Meso-Cenozoic tectonic evolution of the Haiyuan-Liupanshan region, northeastern Tibetan Plateau[J].Journal of Asian earth sciences, 2019, 183(Oct.1):103966.1-103966.13.
[44] Peng H, Wang J, Liu C, et al. Mesozoic exhumation and ca. 10 Ma reactivation of the southern Yin Shan, North China, revealed by low-temperature thermochronology[J]. Tectonophysics, 2022, 823: 229189.
[45] Peng Heng. Fission Track Thermochronology Analysis and Its Geological Significance in the Southwestern Adjacent Area of the Ordos Block[D]. Northwest University, 2020.
[46] Rao G, Chen P, Hu J, et al. Timing of Holocene paleo-earthquakes along the Langshan Piedmont Fault in the western Hetao Graben, North China: Implications for seismic risk[J]. Tectonophysics, 2016, 677: 115-124.
[47] Ren Zhanli, Cui Junping, Qi Kai. New Advances in the Theoretical Research and Methods for Restoring the Thermal Evolution History of Deep and Ultra-deep Layers in Overlapping Basins[J]. Journal of Northwest University (Natural Science Edition), 2022, 52(6): 910-929.
[48] Ren Zhanli, Liu Li, Cui Junping, et al. Application of Tectonic Thermal Evolution History in the Study of Hydrocarbon Accumulation Phases[J]. Oil & Gas Geology, 2008, 29(4): 502-506.
[49] Ren Zhanli, Qi Kai, Liu Runchuan, et al. The Dynamical Background of Early

748 Cretaceous Tectonic Thermal Events in the Ordos Basin and Their Control on the
749 Accumulation Periods of Various Minerals, Including Oil and Gas[J]. Acta
750 Petrologica Sinica, 2020, 36(4): 1213-1234.
751 [50] Ren Zhanli, Tian Tao, Li Jinbu, et al. Research Methods for Thermal Evolution
752 History of Sedimentary Basins and Progress in Reconstructing Thermal Evolution
753 History of Overlapping Basins[J]. Journal of Earth Sciences and Environment, 2014,
754 36(3): 1-20.
755 [51] Ren Zhanli, Yu Qiang, Cui Junping, Qi Kai, Chen Zhanjun, Cao Zhanpeng, Yang
756 Peng. Thermal Evolution History of the Ordos Basin and Its Control on
757 Hydrocarbons[J]. Earth Science Frontiers, 2017, 24(03): 137-148.
758 [52] Ren Zhanli, Zhang Sheng, Gao Shengli, Cui Junping, Xiao Yuanyuan, Xiao Hui.
759 Tectonic Thermal Evolution History of the Ordos Basin and Its Significance for
760 Accumulation and Mineralization[J]. Science in China: Series D, Earth Sciences,
761 2007(S1): 23-32.
762 [53] Ren Zhanli. Study on the Geothermal History of the Ordos Basin Using the
763 Apatite Fission Track Method[J]. Chinese Journal of Geophysics, 1995, 38(03):
764 339-349..
765 [54] Tang Xiyuan, Guo Zhongming, Wang Dingyi. Characteristics, Evolution, and
766 Hydrocarbon Exploration of the Thrust Nappe Structure Belt in the Western Ordos
767 Basin[J]. Oil & Gas Geology, 1988, 9(1): 1-10.
768 [55] Tang Xiyuan. Thrust Nappe Structures and Hydrocarbon Exploration on the
769 Western Margin of the Shaanxi-Gansu-Ningxia Basin[M]. Xi'an: Northwest
770 University Press, 1992.
771 [56] Tapponnier P, XuZ Q, Roger F, et al. 2001. Oblique stepwise riseand growth of
772 the Tibet Plateau. Science, 294(5547):1671-1677.
773 [57] Tian Chaoyang, Chen Hong, Liu Xinshe, et al. Fission Track Ages and Mesozoic
774 Tectonic Uplift in the Niushou Mountain—Luoshan Area of the Western Ordos[J].
775 Journal of Geological Mechanics, 2023, 29(05): 599-617.
776 [58] Vermeesch P. RadialPlotter: A Java application for fission track, luminescence
777 and other radial plots[J]. Radiation Measurements, 2009, 44(4): 409-410.
778 [59] Wang CS, Zhao XX,Liu ZF, et al.2008. Constraints on the earlyuplift history of
779 the Tibetan Plateau, Proc, Natl. Acad. Sci.USA，105(13):4987-4992
780 [60] Yang Hua, Fu Jinhua, Ouyang Zhengjian, Sun Liuyi. Analysis of
781 Tectonic-Sedimentary Environments during the Late Triassic in the Western Margin
782 of the Ordos Basin[J]. Acta Sedimentologica Sinica, 2011, 29(03): 427-439.
783 [61] Yang J.J., Zhang B.R. Basic Characteristics of the Overthrust Belt on the
784 Western Margin of the Ordos Basin[A]. In: Yang J.J., Zhao Z.Y., Liu H.F., et al.
785 Structure and Oil and Gas of the Overthrust Belt on the Western Margin of the Ordos
786 Basin[C]. Lanzhou: Gansu Science and Technology Press, 1990. 91-105.
787 [62] Yang Junjie, Zhang Borong. Strike-Slip Rift and Associated Thrust Belt: A Case
788 Study of the Yinchuan Graben and Hengshanpu Thrust Belt[J]. Petroleum Exploration
789 and Development, 1986(02): 1-8.
790 [63] Yang S.B., Geng X.X., Guo Q.Y., et al. Mesozoic Tectonic Evolution in the
791 Northern Section of the Western Margin of the Ordos Basin[J]. Geological Review,

2008, 54(3): 307-315.
[64] Yang Shengbin, Geng Xinxia, Guo Qingyin, et al. Mesozoic Tectonic Evolution of the Northern Segment of the Western Ordos Basin[J]. Geological Review, 2008, 54(3): 307-315.
[65] Yang Shengbin, Guo Qingyin, Hou Guiting, et al. Subsidence History and Sedimentary Response in the Northern Segment of the Western Ordos Basin[J]. Journal of Peking University: Natural Science Edition, 2006, 42(2): 192-198.
[66] Zhai Mingguo. The Formation, Evolution, and Metallogenesis of the North China Craton[J]. Mineral Deposits, 2010 (1): 24-36.
[67] Zhai Mingguo. The Ordos Block: The Key to Unraveling the Mysteries of Early Continental Formation, Evolution, and Tectonic Regime of the North China Craton[J]. Chinese Science Bulletin, 2021, 66(26): 3441-3461.
[68] Zhang Chengli, Gou Longlong, Liu Xinyu, et al. Precambrian Geological Events, Nature, and Geological Significance of the Basement in the Western North China Craton[J]. Acta Petrologica Sinica, 2018, 34(4): 981-998.
[69] Zhang Guowei, Dong Yunpeng, Yao Anping. A New Starting Point for the Study of Orogenic Belts and Orogenesis[J]. Northwest Geology, 2001, 34(1): 1-9.
[70] Zhang J, Cunningham D, Qu J, et al. Poly-phase structural evolution of the northeastern Alxa Block, China: Constraining the Paleozoic-Recent history of the southern central Asian Orogenic belt[J]. Gondwana Research, 2022, 105: 25-50.
[71] Zhang J, Wang Y, Qu J, et al. Mesozoic intracontinental deformation of the Alxa Block in the middle part of Central Asian Orogenic Belt: A review[J]. International Geology Review, 2021, 63(12): 1490-1520.
[72] Zhang J, Yun L, Zhang B, et al. Deformation at the easternmost Altyn Tagh Fault: Constraints on the growth of the northern Qinghai–Tibetan plateau[J]. Acta Geologica Sinica-English Edition, 2020, 94(4): 988-1006.
[73] Zhang J., Ma Z.J., Ren W.J. Mechanism of North-South Differences in the Overthrust Belt on the Western Margin of the Ordos Basin[J]. Geotectonica et Metallogenia, 2000(02): 124-133.
[74] Zhang Jiasheng, He Zixin, Fei Anqi, et al. Large Margin Thrust Nappe System in the Northern Segment of the Western Ordos Basin[J]. Geological Science, 2008, 43(2): 251-281.
[75] Zhang Jin, Zhang Beihang, Zhao Heng, et al. Characteristics and Mechanisms of Late Cenozoic Deformation in the Beishan-Alashan Region[J]. Earth Science Frontiers, 2023, 30(5): 334.
[76] Zhao Chongyuan, Liu Chiyang, Ren Zhanli. Geology of Oil and Gas Basins and System Engineering in Their Research[J]. Oil & Gas Geology, 1990, 11(1): 108-113.
[77] Zhao D., Chen P., Li R.X., et al. Basin Records of Multistage Tectonic Uplift in the Longshou Mountain of the Northeastern Tibetan Plateau during the Late Cenozoic [J]. Acta Petrologica Sinica, 2023, 39(12): 3759-3774.
[78] Zhao Hongge, Liu Chiyang, Wang Feng, et al. Tectonic Partitioning and Characteristics of the Western Margin of the Ordos Basin[J]. Oil & Gas Geology, 2006, 27(2): 173-179.
[79] Zhao Hongge, Liu Chiyang, Wang Feng, et al. Uplift Timing and Evolution of

the Helan Mountains[J]. Science in China: Series D, 2007, 37(A01): 185-192.
[80] Zhao Hongge, Liu Chiyang, Wang Jianqiang, et al. Exploration of Tectonic Attributes during the Late Triassic in the Western Ordos Basin[J]. Geological Journal of China, 2007, 34(3): 384-391.
[81] Zhao Hongge, Liu Chiyang, Yao Yaming, Wang Feng, Yin Yan. Fission Track Evidence of Differential Uplift in the Western Ordos Basin[J]. Journal of Northwest University (Natural Science Edition), 2007, (03): 470-474.
[82] Zhao Hongge. Tectonic Characteristics and Evolution of the Western Ordos Basin[D]. Northwest University, 2003.
[83] Zhao Pan, Xu Bei, Chen Yan. Mongolian–Okhotsk Ocean: Evolutionary Process and Final Closure[J]. Science in China: Earth Sciences, 2023, 53(11): 2541-2559.
[84] Zhao X, Coe R S. 1987.Palaeomagnetic constraints on the collision and rotation of North and SouthChina. Nature, 327:41-144.
[85] Zhao Xiaochen. Mesozoic Tectonic Evolution and Later Modification of the Northern Section of the North-South Tectonic Belt in China[D]. Xi'an: Northwest University, 2017.
[86] Zhao Y, Liu X, Hu J, et al. Metamorphism of diverse basement gneisses of the Ordos Basin: Record of multistage Paleoproterozoic orogenesis and constraints on the evolution of the western North China Craton[J]. Precambrian Research, 2019, 328: 48-63.
[87] Zhuo Yuzhou. Determination of Mesozoic-Cenozoic Uplift Events in the Zhuozishan Area of the Northwestern Ordos Basin and Their Tectonic Significance[D]. Northwest University, 2015.